Smart Structures and Systems, *Vol. 30, No. 3 (2022) 221-237*
https://doi.org/10.12989/sss.2022.30.3.221

Modeling and numerical simulation of electrostrictive materials and structures

Astrid Pechstein [a], Michael Krommer* and Alexander Humer [b]

Institute of Technical Mechanics, Johannes Kepler University Linz, Altenberger Straße 69, 4040 Linz, Austria

(*Received December 26, 2015, Revised January 2, 2016, Accepted January 15, 2016*)

Abstract. This paper is concerned with nonlinear modeling and efficient numerical simulation of electrostrictive materials and structures. Two types of such materials are considered: relaxor ferroelectric ceramics and electrostrictive polymers. For ceramics, a geometrically linear formulation is developed, whereas polymers are studied in a geometrically nonlinear regime. In the paper, we focus on constitutive modeling first. For the reversible constitutive response under consideration, we introduce the augmented Helmholtz free energy, which is composed of a purely elastic part, a dielectric part and an augmentation term. For the elastic part, we involve an additive decomposition of the strain tensor into an elastic strain and an electrostrictive eigenstrain, which depends on the polarization of the material. In the geometrically nonlinear case, a corresponding multiplicative decomposition of the deformation gradient tensor replaces the additive strain decomposition used in the geometrically linear formulation. For the dielectric part, we first introduce the internal energy, to which a Legendre transformation is applied to compute the free energy. The augmentation term accounts for the contribution from vacuum to the energy. In our formulation, the augmented free energy depends not only on the strain and the electric field, but also on the polarization and an internal polarization; the latter two are internal variables. With the constitutive framework established, a Finite Element implementation is briefly discussed. We use high-order elements for the discretization of the independent variables, which include also the internal variables and, in case the material is assumed incompressible, the hydrostatic pressure, which is introduced as a Lagrange multiplier. The elements are implemented in the open source code Netgen/NGSolve. Finally, example problems are solved for both, relaxor ferroelectric ceramics and electrostrictive polymers. We focus on thin plate-type structures to show the efficiency of the numerical scheme and its applicability to thin electrostrictive structures.

Keywords: electrostrictive polymers; Finite Element method; geometrical and physical nonlinearity; numerical simulation; polarization saturation; relaxor ferroelectric ceramics

1. Introduction

So-called smart materials react to different stimuli, which requires a deepened understanding of the multi-physics coupling in these materials. To support real world applications of smart materials and structures an efficient and accurate modeling able to capture all relevant coupling effects and nonlinearities is important for the optimal design of material properties or the optimal spatial distribution of the smart materials in a mechanical system, see e.g. (Goncalves *et al*. 2016, Amini *et al*. 2020, Cao *et al*. 2021) for control and optimal design of smart structures embodying widely used piezoelectric materials.

Among many others, piezoelectric materials are smart materials that are reactive to electrical stimuli. In the present paper, we focus on this type of smart materials, i.e., on so-called electro-active materials, for which we discuss modeling approaches within a classical continuum physics approach. The basics of nonlinear electro-elasticity date back to Toupin (1956) with further developments by e.g. Pao (1978), Prechtl (1982a,b) and Maugin (1998). A special case, to which the theory of nonlinear electro-elasticity is applicable are so-called elastic dielectrics. Modeling of the latter involves the concept of the total stress tensor and the so-called augmented free energy to account for ponderomotive forces. In addition, constitutive coupling through effects like piezoelectricity and electrostriction is present and must be account for; typically, by accounting for both mechanical and electrical contributions in the Helmholtz free energy, see among others Pao (1978), Dorfmann and Ogden (2005) and Gao *et al*. (2011).

In the present contribution, we focus on the specific case of electro-active materials exhibiting electrostriction. We study two classes; relaxor ferroelectric ceramics and electrostrictive polymers. In general, electro-active materials can be classified into dielectric materials, electrostrictive materials and ferroelectric materials, see Pelrine *et al*. (1998) or Bar-Cohen (2004) for this classification in the case of electro-active polymers and Mukherjee and Ganguli (2010) or Moghadam *et al*. (2015) for applications of electro-active polymers. We understand dielectric materials as materials actuated through electro-static and ponderomotive forces only, ferroelectric materials as materials exhibiting an electrostrictive effect in a non-poled virgin state, but showing piezoelectric behavior in the poled state, and electrostrictive materials as materials actuated by both, electrostatic and pondermotive forces as

*Corresponding author, Professor,
E-mail: michael.krommer@jku.at
[a] Associate Professor, E-mail: astrid.pechstein@jku.at
[b] Associate Professor, E-mail: alexander.humer@jku.at

ISSN: 1738-1584 (Print), 1738-1991 (Online)

well as through electrostriction, see Kamlah (2001) for a detailed discussion of these different types of electro-active materials. Otherwise, there is a vast amount of literature on modeling, simulation and experimentation of electro-active materials and structures; e.g., Hom and Shankar (1994), McMeeking and Landis (2005), Dorfmann and Ogden (2005), Klinkel (2006), Vu *et al*. (2007), Diaconu *et al*. (2008), Ask *et al*. (2012), Klinkel *et al*. (2013), Yang *et al*. (2013), Humer and Krommer (2015), Zäh and Miehe (2015), Mehnert *et al*. (2016), Katsouras *et al*. (2016), Vetyukov *et al*. (2018), Hansy-Staudigl *et al*. (2019), Pechstein (2019), Humer *et al*. (2020), Hansy-Staudigl and Krommer (2021) and Pechstein *et al*. (2021) to mention just a few contributions.

When it comes to ferroelectric or electrostrictive materials, constitutive coupling becomes relevant, and the Helmholtz free energy must account for coupling effects, in particular electrostriction and piezoelectricity. Many different approaches towards the modeling of electrostrictive coupling have been reported in the literature. These range from the simplest model of a deformation-dependent permittivity, Suo (2010), to more advanced models using either additional terms in the free energy, see e.g. Mehnert *et al*. (2016), in which combined electromechanical invariants were introduced, or classical decomposition methods well established in many other fields of inelasticity. Prominent examples are thermoelasticity, elastoplasticity and viscoelasticity, see Lubarda (2004) for a review and Bonet (2001) for large strain viscoelasticity, as well as the field of micromechanics of defects, see Mura (1987). For electro-elastic continua at finite strains a multiplicative decomposition of the deformation gradient tensor into a purely elastic and a purely electrical part is typically applied. Such a multiplicative decomposition of the deformation gradient tensor resembles a consistent extension of the classical additive decomposition of the strain tensor, used in the small deformation regime, to large deformations. The additive decomposition of the total strain tensor into an elastic part and an inelastic part (also denoted as eigenstrain) was introduced in the famous paper by Reissner (1931). In the context of electro-elasticity the additive decomposition is used with the objective to incorporate eigenstrains of electrical origin; e.g., for the modeling of piezoelectric materials in the framework of Voigt's linearized theory of piezoelectricity, for the modeling of ferroelectric and ferroelastic hysteresis, see Kamlah (2001), but also for modeling electrostriction in the small deformation regime, see Su *et al*. (1999) for the definition of the electrostrictive eigenstrain and the eigenstrain due to the so-called Maxwell effect. Moving back to the context of finite strain electro-elasticity a multiplicative decomposition of the deformation gradient tensor has already been used for piezoelectric materials as well as ferroelectric materials and electrostrictive polymers, see Humer and Krommer (2015), Zäh and Miehe (2015), Humer *et al*. (2020), Hansy-Staudigl and Krommer (2021) and Skatulla *et al*. (2012). In other words, it represents a framework for constitutive modeling of electro-active materials and it enables both, a phenomenological approach as well as an approach based on the microstructure of the materials. Note that the references concerning finite strain electro-elasticity consider electro-active polymers as electro-elastic, rather than – more realistically – as electro-viscoelastic. For the latter case see Ask *et al*. (2012), in which the multiplicative decomposition is used to account for the viscous parts of the deformation gradient tensor, while electrostriction is taken into account additively in the augmented free energy. Nevertheless, in the present paper, we also remain within the framework of electro-elasticity leaving the extension to a multi-multiplicative decomposition needed for electro-viscoelasticity for future work. In other words, we only study the long-term or steady state response of electrostrictive materials and structures. Also, we point out that we have discussed modeling approaches for both, ferroelectric materials and electrostrictive materials in this paragraph, because we understand electrostrictive materials as ferroelectric materials, for which the coercive field strength and the so-called driving force are zero and no piezoelectric effect occurs. The constitutive response is reversible and the material behaves as a relaxor ferroelectric only exhibiting reversible electrostriction. This approach is applicable for both, relaxor ferroelectric ceramics and polymers as discussed in Hom and Shankar (1994) and Yang *et al*. (2013) as well as electrostrictive polymers.

The present paper is structured as follows. After this general introduction, the constitutive framework for electrostrictive materials is discussed in detail in Section 2. Then, we give a short brief on the implementation of an efficient Finite Element schema in Section 3, which is used in Section 4 to compute numerical solutions to selected example problems. A conclusion completes the paper.

2. Constitutive framework

We start our discussion of constitutive equations of elastic dielectrics by introducing a thermodynamic potential Ω per unit volume of a (undeformed) reference configuration, the time derivative of which is

$$\dot{\Omega} = \mathbf{S} \cdot \cdot \dot{\mathbf{E}} - \boldsymbol{\mathcal{D}} \cdot \dot{\boldsymbol{\mathcal{E}}}, \tag{1}$$

see Eringen and Maugin (1990). Hence, we are discussing reversible constitutive processes. We use standard notation in defining the displacement vector $\boldsymbol{u}$ and the deformation gradient tensor $\mathbf{F} = \mathbf{I} + \nabla \boldsymbol{u}$, where ∇ is the nabla operator of the reference configuration. With the right Cauchy-Green tensor $\mathbf{C} = \mathbf{F}^T \cdot \mathbf{F}$, the Green strain tensor is defined as $\mathbf{E} = 1/2(\mathbf{C} - \mathbf{I})$. The material electric field vector is denoted by $\boldsymbol{\mathcal{E}}$, which is related to the spatial electric field vector $\boldsymbol{e}$ by $\boldsymbol{\mathcal{E}} = \mathbf{F}^T \cdot \boldsymbol{e}$. The work conjugate entities $\mathbf{S}$ and $\boldsymbol{\mathcal{D}}$ are the total second Piola-Kirchhoff stress tensor and the material electric displacement vector. The independent variables of the thermodynamic potential follow from Eq. (1) as $\mathbf{E}$ or alternatively $\mathbf{C}$ and $\boldsymbol{\mathcal{E}}$. Therefore, the thermodynamic potential is introduced as $\Omega(\mathbf{C}, \boldsymbol{\mathcal{E}})$. Often, Ω is referred to as the augmented Helmholtz free energy, which is composed of the free energy $\Phi(\mathbf{C}, \boldsymbol{\mathcal{E}})$ and an augmentation potential, in which ε_0 denotes the permittivity in vacuum

$$\Omega(\mathbf{C},\boldsymbol{\mathcal{E}}) = \Phi(\mathbf{C},\boldsymbol{\mathcal{E}}) + \Phi_0(\mathbf{C},\boldsymbol{\mathcal{E}}),$$
$$\Phi_0 = -\frac{1}{2}\varepsilon_0 J\boldsymbol{\mathcal{E}}\cdot(\mathbf{C}^{-1}\cdot\boldsymbol{\mathcal{E}}). \tag{2}$$

Above, $J = \det\mathbf{F}$ denotes the determinant of the deformation gradient tensor $\mathbf{F}$. Then, $\mathbf{S}$ and $\boldsymbol{\mathcal{D}}$ follow to

$$\mathbf{S} = 2\frac{\partial\Omega}{\partial\mathbf{C}}, \quad \boldsymbol{\mathcal{D}} = -\frac{\partial\Omega}{\partial\boldsymbol{\mathcal{E}}}. \tag{3}$$

The material electric displacement vector can be written as $\boldsymbol{\mathcal{D}} = \varepsilon_0 J\mathbf{C}^{-1}\cdot\boldsymbol{\mathcal{E}} + \boldsymbol{\mathcal{P}}$, in which the material polarization vector $\boldsymbol{\mathcal{P}}$ is the negative derivative of the free energy $\Phi(\mathbf{C},\boldsymbol{\mathcal{E}})$ with respect to $\boldsymbol{\mathcal{E}}$. The total stress tensor is composed of a mechanical part $\mathbf{S}_{\mathrm{me}}$ and a so-called ponderomotive stress tensor $\mathbf{S}_{\mathrm{pon}}$

$$\begin{aligned}\mathbf{S}_{\mathrm{pon}} &= \left(\boldsymbol{\mathcal{D}}\boldsymbol{\mathcal{E}} - \frac{1}{2}\varepsilon_0 J\mathbf{C}^{-1}(\boldsymbol{\mathcal{E}}\cdot\boldsymbol{\mathcal{E}})\right)\cdot\mathbf{C}^{-1}\\ &= \boldsymbol{\mathcal{P}}\boldsymbol{\mathcal{E}}\cdot\mathbf{C}^{-1} + \mathbf{S}_{\mathrm{M}}.\end{aligned} \tag{4}$$

Note that the divergence of the ponderomotive stress tensor is the ponderomotive body force vector, see Dorfmann and Ogden (2005), Mehnert *et al*. (2016) and Bustamante (2009). Moreover, the ponderomotive stress tensor is composed of a polarization stress tensor $\mathbf{S}_{\mathrm{pol}} = \boldsymbol{\mathcal{P}}\boldsymbol{\mathcal{E}}\cdot\mathbf{C}^{-1}$ and the famous Maxwell stress tensor $\mathbf{S}_{\mathrm{M}}$

$$\mathbf{S}_{\mathrm{M}} = \left(\varepsilon_0 J\mathbf{C}^{-1}\cdot\boldsymbol{\mathcal{E}}\boldsymbol{\mathcal{E}} - \frac{1}{2}\varepsilon_0 J\mathbf{C}^{-1}(\boldsymbol{\mathcal{E}}\cdot\boldsymbol{\mathcal{E}})\right)\cdot\mathbf{C}^{-1}. \tag{5}$$

The Maxwell stress tensor is twice the derivative of the augmentation energy Φ_0 with respect to $\mathbf{C}$, while the sum of the mechanical stress tensor and the polarization stress tensor $\mathbf{S}_{\mathrm{S}} = \mathbf{S}_{\mathrm{me}} + \mathbf{S}_{\mathrm{pol}}$, which is symmetric, is twice the derivative of the free energy $\Phi(\mathbf{C},\boldsymbol{\mathcal{E}})$ with respect to $\mathbf{C}$. The constitutive relations are valid for elastic dielectrica in general, as long as no irreversible constitutive processes occur. Electrostrictive materials that will be studied as a particular material in this paper belong to this class of materials.

2.1 Relaxor ferroelectric ceramics

As a first class of electrostrictive materials, we consider relaxor ferroelectric ceramics. For small deformations and electric fields as observed in relaxor ferroelectric ceramics the augmented free energy is approximated by

$$\Omega(\boldsymbol{\varepsilon},\boldsymbol{\mathcal{E}}) = \Phi(\boldsymbol{\varepsilon},\boldsymbol{\mathcal{E}}) - \frac{1}{2}\varepsilon_0\boldsymbol{\mathcal{E}}\cdot\boldsymbol{\mathcal{E}}, \tag{6}$$

in which the transformation between the material and the spatial electric field vector and the transformation between volume elements have been neglected in the augmentation potential, $\boldsymbol{\mathcal{E}} \approx \boldsymbol{e}$ and $J \approx 1$. The free energy is formulated in terms of the linearized strain tensor $\boldsymbol{\varepsilon} = \frac{1}{2}(\nabla\boldsymbol{u} + (\nabla\boldsymbol{u})^T)$ rather than in terms of the right Cauchy-Green tensor $\mathbf{C}$.

Next, the free energy is additively decomposed into an elastic part Φ_{e} and a dielectric part Φ_d; hence, $\Phi = \Phi_{\mathrm{e}} + \Phi_{\mathrm{d}}$. We introduce the elastic part as

$$\Phi_{\mathrm{e}}(\boldsymbol{\varepsilon}_{\mathrm{e}}) = \frac{1}{2}\boldsymbol{\varepsilon}_{\mathrm{e}}\cdot\cdot\,\mathbb{C}\cdot\cdot\,\boldsymbol{\varepsilon}_{\mathrm{e}}, \tag{7}$$

in which we have used the additive decomposition $\boldsymbol{\varepsilon} = \boldsymbol{\varepsilon}_e + \boldsymbol{\varepsilon}^*$ of the strain tensor into an elastic part $\boldsymbol{\varepsilon}_{\mathrm{e}}$ and an electrostrictive eigenstrain $\boldsymbol{\varepsilon}^*$. $\mathbb{C}$ is the fourth rank elasticity tensor. In order to introduce the dielectric part, we start with the internal energy, in which we account for a nonlinear and a linear dielectric response

$$e = \Psi(\boldsymbol{\mathcal{P}}_{\mathrm{i}}) + \frac{1}{2}(\boldsymbol{\mathcal{P}} - \boldsymbol{\mathcal{P}}_{\mathrm{i}})\cdot(\varepsilon_0\boldsymbol{\chi}_0)^{-1}\cdot(\boldsymbol{\mathcal{P}} - \boldsymbol{\mathcal{P}}_{\mathrm{i}}), \tag{8}$$

with the vacuum permittivity ε_0, the polarization vector $\boldsymbol{\mathcal{P}}$, a second rank susceptibility tensor $\boldsymbol{\chi}_0$ and an internal polarization vector $\boldsymbol{\mathcal{P}}_{\mathrm{i}}$. The Legendre transformation $\Phi_d = e - \boldsymbol{\mathcal{E}}\cdot\boldsymbol{\mathcal{P}}$ results into

$$\begin{aligned}\Phi_{\mathrm{d}} = \Psi(\boldsymbol{\mathcal{P}}_{\mathrm{i}}) &+ \frac{1}{2}(\boldsymbol{\mathcal{P}} - \boldsymbol{\mathcal{P}}_{\mathrm{i}})\cdot(\varepsilon_0\boldsymbol{\chi}_0)^{-1}\\ &\cdot(\boldsymbol{\mathcal{P}} - \boldsymbol{\mathcal{P}}_{\mathrm{i}}) - \boldsymbol{\mathcal{E}}\cdot\boldsymbol{\mathcal{P}},\end{aligned} \tag{9}$$

such that the augmented free energy takes the form

$$\begin{aligned}\Omega(\boldsymbol{\varepsilon},\boldsymbol{\mathcal{E}},\boldsymbol{\mathcal{P}},\boldsymbol{\mathcal{P}}_{\mathrm{i}}) = &\frac{1}{2}\boldsymbol{\varepsilon}_{\mathrm{e}}\cdot\cdot\,\mathbb{C}\cdot\cdot\,\boldsymbol{\varepsilon}_{\mathrm{e}} + \Psi(\boldsymbol{\mathcal{P}}_{\mathrm{i}})\\ &+\frac{1}{2}(\boldsymbol{\mathcal{P}} - \boldsymbol{\mathcal{P}}_{\mathrm{i}})\cdot(\varepsilon_0\boldsymbol{\chi}_0)^{-1}\cdot(\boldsymbol{\mathcal{P}} - \boldsymbol{\mathcal{P}}_{\mathrm{i}})\\ &-\boldsymbol{\mathcal{E}}\cdot\boldsymbol{\mathcal{P}} - \frac{1}{2}\varepsilon_0\boldsymbol{\mathcal{E}}\cdot\boldsymbol{\mathcal{E}}.\end{aligned} \tag{10}$$

In this formulation combining a linear with a nonlinear dielectric response, the augmented free energy depends on the strain tensor $\boldsymbol{\varepsilon}$, the electric field vector $\boldsymbol{\mathcal{E}}$, the polarization vector $\boldsymbol{\mathcal{P}}$ and an internal polarization $\boldsymbol{\mathcal{P}}_{\mathrm{i}}$. The eigenstrain accounts for electrostriction and it is therefore assumed as $\boldsymbol{\varepsilon}^* = \boldsymbol{\varepsilon}^*(\boldsymbol{\mathcal{P}})$. From the time derivative of the augmented free energy,

$$\begin{aligned}\dot{\Omega} &= \frac{\partial\Omega}{\partial\boldsymbol{\varepsilon}}\cdot\cdot\,\dot{\boldsymbol{\varepsilon}} + \frac{\partial\Omega}{\partial\boldsymbol{\mathcal{E}}}\cdot\dot{\boldsymbol{\mathcal{E}}} + \frac{\partial\Omega}{\partial\boldsymbol{\mathcal{P}}}\cdot\dot{\boldsymbol{\mathcal{P}}} + \frac{\partial\Omega}{\partial\boldsymbol{\mathcal{P}}_{\mathrm{i}}}\cdot\dot{\boldsymbol{\mathcal{P}}}_{\mathrm{i}}\\ &= \boldsymbol{\sigma}\cdot\cdot\,\dot{\boldsymbol{\varepsilon}} - \boldsymbol{\mathcal{D}}\cdot\dot{\boldsymbol{\mathcal{E}}},\end{aligned} \tag{11}$$

we obtain the stress tensor $\boldsymbol{\sigma}$ and the electric displacement vector $\boldsymbol{\mathcal{D}}$ as

$$\begin{aligned}\boldsymbol{\sigma} &= \frac{\partial\Omega}{\partial\boldsymbol{\varepsilon}} = \mathbb{C}\cdot\cdot\,\boldsymbol{\varepsilon}_{\mathrm{e}} = \mathbb{C}\cdot\cdot\,(\boldsymbol{\varepsilon} - \boldsymbol{\varepsilon}^*),\\ \boldsymbol{\mathcal{D}} &= -\frac{\partial\Omega}{\partial\boldsymbol{\mathcal{E}}} = \varepsilon_0\boldsymbol{\mathcal{E}} + \boldsymbol{\mathcal{P}},\end{aligned} \tag{12}$$

which represent the classical constitutive relations. The derivatives of the augmented free energy with respect to $\boldsymbol{\mathcal{P}}$ and $\boldsymbol{\mathcal{P}}_{\mathrm{i}}$

$$\frac{\partial\Omega}{\partial\boldsymbol{\mathcal{P}}} = -\boldsymbol{\mathcal{E}} + (\varepsilon_0\boldsymbol{\chi}_0)^{-1}\cdot(\boldsymbol{\mathcal{P}} - \boldsymbol{\mathcal{P}}_{\mathrm{i}}) - \boldsymbol{\sigma}\cdot\cdot\,\frac{\partial\boldsymbol{\varepsilon}^*}{\partial\boldsymbol{\mathcal{P}}} = \mathbf{0}, \tag{13}$$

$$\frac{\partial\Omega}{\partial\boldsymbol{\mathcal{P}}_{\mathrm{i}}} = \frac{\partial\Psi}{\partial\boldsymbol{\mathcal{P}}_{\mathrm{i}}} - (\varepsilon_0\boldsymbol{\chi}_0)^{-1}\cdot(\boldsymbol{\mathcal{P}} - \boldsymbol{\mathcal{P}}_{\mathrm{i}}) = \mathbf{0}, \tag{14}$$

must vanish, because $\boldsymbol{\mathcal{P}}$ and $\boldsymbol{\mathcal{P}}_\mathrm{i}$ have the role of internal variables in the augmented free energy, such that their work conjugates must vanish. The resulting relations represent algebraic equations between the electric field, the polarization, the internal polarization and the stress.

In case the susceptibility $\boldsymbol{\chi}_0$ is negligible as compared to the respective contribution from Ψ, we may set $\boldsymbol{\mathcal{P}}_\mathrm{i} = \boldsymbol{\mathcal{P}}$, and the augmented free energy simplifies to

$$\begin{aligned}\Omega(\boldsymbol{\varepsilon}, \boldsymbol{\mathcal{E}}, \boldsymbol{\mathcal{P}}) = \frac{1}{2}\boldsymbol{\varepsilon}_\mathrm{e} \cdot\cdot\, \mathbb{C} \cdot\cdot\, \boldsymbol{\varepsilon}_\mathrm{e} + \Psi(\boldsymbol{\mathcal{P}}) \\ -\boldsymbol{\mathcal{E}} \cdot \boldsymbol{\mathcal{P}} - \frac{1}{2}\varepsilon_0 \boldsymbol{\mathcal{E}} \cdot \boldsymbol{\mathcal{E}}.\end{aligned} \tag{15}$$

The constitutive relations become

$$\boldsymbol{\sigma} = \frac{\partial \Omega}{\partial \boldsymbol{\varepsilon}} = \mathbb{C} \cdot\cdot\, \boldsymbol{\varepsilon}_\mathrm{e} = \mathbb{C} \cdot\cdot\, (\boldsymbol{\varepsilon} - \boldsymbol{\varepsilon}^*), \tag{16}$$

$$\boldsymbol{\mathcal{D}} = -\frac{\partial \Omega}{\partial \boldsymbol{\mathcal{E}}} = \varepsilon_0 \boldsymbol{\mathcal{E}} + \boldsymbol{\mathcal{P}}, \tag{17}$$

$$\boldsymbol{\mathcal{E}} = \frac{\partial \Psi}{\partial \boldsymbol{\mathcal{P}}} - \boldsymbol{\sigma} \cdot\cdot\, \frac{\partial \boldsymbol{\varepsilon}^*}{\partial \boldsymbol{\mathcal{P}}} = \frac{\partial (\Phi + \boldsymbol{\mathcal{E}} \cdot \boldsymbol{\mathcal{P}})}{\partial \boldsymbol{\mathcal{P}}}. \tag{18}$$

In the last relation above, $\Phi + \boldsymbol{\mathcal{E}} \cdot \boldsymbol{\mathcal{P}}$ results from a partial Legendre transformation. The latter formulation has been used in the literature on relaxor ferroelectric ceramics, see Hom and Shankar (1994).

2.1.1 Isotropic relaxor ferroelectric ceramics

As a special case we consider isotropic relaxor ferroelectric ceramics, for which the augmented free energy is

$$\begin{aligned}\Omega = \mu \boldsymbol{\varepsilon}_\mathrm{e} \cdot\cdot\, \boldsymbol{\varepsilon}_\mathrm{e} + \frac{\lambda}{2}(\mathrm{tr}\boldsymbol{\varepsilon}_\mathrm{e})^2 + \Psi(\boldsymbol{\mathcal{P}}_\mathrm{i}) \\ + \frac{1}{2}\frac{1}{\varepsilon_0 \chi_0}(\boldsymbol{\mathcal{P}} - \boldsymbol{\mathcal{P}}_\mathrm{i}) \cdot (\boldsymbol{\mathcal{P}} - \boldsymbol{\mathcal{P}}_\mathrm{i}) - \boldsymbol{\mathcal{E}} \cdot \boldsymbol{\mathcal{P}} - \frac{1}{2}\varepsilon_0 \boldsymbol{\mathcal{E}} \cdot \boldsymbol{\mathcal{E}},\end{aligned} \tag{19}$$

with $\boldsymbol{\varepsilon}_e = \boldsymbol{\varepsilon} - \boldsymbol{\varepsilon}^*$ and the Lamé parameters μ and λ. We introduce the electrostrictive eigenstrain as $\boldsymbol{\varepsilon}^* = \mathbb{Q} \cdot\cdot\, \boldsymbol{\mathcal{P}}\boldsymbol{\mathcal{P}}$ with an isotropic fourth rank electrostrictive tensor $\mathbb{Q}$, such that

$$\boldsymbol{\varepsilon}^* = Q\left(\left(1 + \nu_\mathrm{Q}\right)\boldsymbol{\mathcal{P}}\boldsymbol{\mathcal{P}} - \nu_\mathrm{Q}\mathbf{I}(\boldsymbol{\mathcal{P}} \cdot \boldsymbol{\mathcal{P}})\right), \tag{20}$$

with the electrostrictive coefficient Q and an electrostrictive Poisson ratio ν_Q. For an incompressible eigenstrain with $\nu_\mathrm{Q} = 0.5$ this reduces to

$$\boldsymbol{\varepsilon}^* = \frac{3}{2}Q\left(\boldsymbol{\mathcal{P}}\boldsymbol{\mathcal{P}} - \frac{1}{3}\mathbf{I}(\boldsymbol{\mathcal{P}} \cdot \boldsymbol{\mathcal{P}})\right). \tag{21}$$

Finally, the potential $\Psi(\boldsymbol{\mathcal{P}}_\mathrm{i})$ must be specified. For the isotropic material we choose $\Psi = \Psi(\|\boldsymbol{\mathcal{P}}_\mathrm{i}\|)$, such that its derivative is

$$\begin{aligned}&\frac{\partial \Psi}{\partial \boldsymbol{\mathcal{P}}_\mathrm{i}} = \frac{\partial \Psi(\|\boldsymbol{\mathcal{P}}_\mathrm{i}\|)}{\partial \|\boldsymbol{\mathcal{P}}_\mathrm{i}\|}\frac{\partial \|\boldsymbol{\mathcal{P}}_\mathrm{i}\|}{\partial \boldsymbol{\mathcal{P}}_\mathrm{i}} = \Psi'(\|\boldsymbol{\mathcal{P}}_\mathrm{i}\|)\frac{\boldsymbol{\mathcal{P}}_\mathrm{i}}{\|\boldsymbol{\mathcal{P}}_\mathrm{i}\|} \\ &\text{with}\quad \Psi'(\|\boldsymbol{\mathcal{P}}_\mathrm{i}\|) = \frac{\mathcal{P}_\mathrm{sat}^n}{2\varepsilon_0 \chi_\mathrm{i}(n-1)}((\mathcal{P}_\mathrm{sat} - \|\boldsymbol{\mathcal{P}}_\mathrm{i}\|)^{1-n} \\ &\qquad - (\mathcal{P}_\mathrm{sat} + \|\boldsymbol{\mathcal{P}}_\mathrm{i}\|)^{1-n}),\end{aligned} \tag{22}$$

with χ_i a susceptibility, $\mathcal{P}_\mathrm{sat}$ the saturation polarization and n a shape parameter. This family of potentials is also used for ferroelectric ceramics, see Pechstein *et al*. (2021). The conditions

$$\begin{aligned}&\|\boldsymbol{\mathcal{P}}_\mathrm{i}\| \leq \mathcal{P}_\mathrm{sat}, \quad \Psi'|_{\|\boldsymbol{\mathcal{P}}_\mathrm{i}\|=0} = 0, \quad \lim_{\|\boldsymbol{\mathcal{P}}_\mathrm{i}\| \to \mathcal{P}_\mathrm{sat}} \Psi' = \infty, \\ &\Psi''|_{\|\boldsymbol{\mathcal{P}}_\mathrm{i}\|=0} = \frac{1}{\varepsilon_0 \chi_\mathrm{i}}, \qquad \Psi'' \geq \frac{1}{\varepsilon_0 \chi_\mathrm{i}}\end{aligned} \tag{23}$$

are satisfied.

2.1.2 Homogenous deformation of a disc

As a simple test for the validity of the present formulation, we study a homogenous isotropic disc of thickness H with electrodes at the upper and lower side. The lower electrode is grounded and an electric potential V is applied at the upper electrode. No external forces act, such that the stress tensor is trivial, $\boldsymbol{\sigma} = \mathbf{0}$. Therefore, the strain is equal to the electrostrictive eigenstrain

$$\boldsymbol{\varepsilon} = \boldsymbol{\varepsilon}^* = Q\left(\left(1 + \nu_\mathrm{Q}\right)\boldsymbol{\mathcal{P}}\boldsymbol{\mathcal{P}} - \nu_\mathrm{Q}\mathbf{I}(\boldsymbol{\mathcal{P}} \cdot \boldsymbol{\mathcal{P}})\right). \tag{24}$$

For this problem a homogenous deformation occurs and the electric field vector, the polarization vector and the internal polarization vector have only a homogenous thickness component; hence, $\boldsymbol{\mathcal{E}} = \mathcal{E}\boldsymbol{e}_3 = VH^{-1}\boldsymbol{e}_3$, $\boldsymbol{\mathcal{P}} = \mathcal{P}\boldsymbol{e}_3$ and $\boldsymbol{\mathcal{P}}_\mathrm{i} = \mathcal{P}_\mathrm{i}\boldsymbol{e}_3$ hold with the unit vector in thickness direction $\boldsymbol{e}_3$. Then, the polarization and the internal polarization can be computed from

$$\begin{aligned}-\mathcal{E} + \frac{1}{\varepsilon_0 \chi_0}(\mathcal{P} - \mathcal{P}_\mathrm{i}) = 0, \\ \frac{\partial \Psi}{\partial \mathcal{P}_\mathrm{i}} - \frac{1}{\varepsilon_0 \chi_0}(\mathcal{P} - \mathcal{P}_\mathrm{i}) = 0.\end{aligned} \tag{25}$$

Hence, $\mathcal{P}_\mathrm{i}$ is implicitely defined via

$$\mathcal{E} = \frac{\partial \Psi}{\partial \mathcal{P}_\mathrm{i}}, \tag{26}$$

and the polarization becomes

$$\mathcal{P} = \varepsilon_0 \chi_0 \mathcal{E} + \mathcal{P}_\mathrm{i}. \tag{27}$$

We consider the case $n = 1$ in the potential Ψ, for which we obtain

$$\begin{aligned}\mathcal{E} &= \frac{\mathcal{P}_\mathrm{sat}}{2\varepsilon_0 \chi_\mathrm{i}}\frac{\mathcal{P}_\mathrm{i}}{|\mathcal{P}_\mathrm{i}|}\left(\ln\left(\frac{\mathcal{P}_\mathrm{sat} + |\mathcal{P}_\mathrm{i}|}{\mathcal{P}_\mathrm{sat} - |\mathcal{P}_\mathrm{i}|}\right)\right) \\ &= \frac{\mathcal{P}_\mathrm{sat}}{\varepsilon_0 \chi_\mathrm{i}}\mathrm{arctanh}\left(\frac{|\mathcal{P}_\mathrm{i}|}{\mathcal{P}_\mathrm{sat}}\right)\frac{\mathcal{P}_\mathrm{i}}{|\mathcal{P}_\mathrm{i}|}.\end{aligned} \tag{28}$$

The normal strain in thickness direction is

$$\varepsilon_{33} = \boldsymbol{e}_3 \cdot \boldsymbol{\varepsilon}^* \cdot \boldsymbol{e}_3 = Q\left(\left(1 + \nu_\mathrm{Q}\right)\boldsymbol{\mathcal{P}}^2 - \nu_\mathrm{Q}\boldsymbol{\mathcal{P}}^2\right) = Q\mathcal{P}^2; \tag{29}$$

ε_{33} is independent from the electrostrictive Poisson ratio ν_Q. Finally, we note that for a small internal polarization the linearized relation between electric field and internal polarization is $\mathcal{P}_\mathrm{i} = \varepsilon_0 \chi_\mathrm{i} \mathcal{E}$ and the electrostrictive eigenstrain becomes

Table 1 Material parameters for a PMN-PT-BT relaxor ferroelectric at 5°C taken from (Hom and Shankar 1994)

Y/Nm^2	$Q_{111}/\mathrm{m}^4\mathrm{C}^{-2}$	$Q_{122}/\mathrm{m}^4\mathrm{C}^{-2}$	$\mathcal{P}_{\mathrm{sat}}/\mathrm{Cm}^{-2}$	k/mV^{-1}
97×10^9	13.3×10^{-3}	-6.06×10^{-3}	0.259	1.16×10^{-6}

$$\varepsilon_{33} = Q\mathcal{P}^2 = Q\varepsilon_0^2(\chi_0+\chi_\mathrm{i})^2\mathcal{E}^2, \tag{30}$$

which is in full agreement with classical formulations for electrostriction, see e.g., Su *et al*. (1999). Note that the Maxwell contribution is not accounted for in this small strain formulation.

To present numerical results, we use the material parameters for a PMN-PT-BT relaxor ferroelectric at 5°C taken from Hom and Shankar (1994), which are given in Table 1. These material parameters are related to the ones used in our formulation by means of $Q = Q_{111}$, $Qv_\mathrm{Q} = -Q_{122}$ and $\varepsilon_0\chi_\mathrm{i} = \mathcal{P}_{\mathrm{sat}}k$; also, note $\chi_0 = 0$ such that $\mathcal{P} = \mathcal{P}_\mathrm{i}$. Therefore, $\mathcal{P}$ fellows directly from Eq. (28). The numerical results are presented in Fig. 1, in which the data from Hom and Shankar (1994) is also shown (circular markers).

2.2 Isotropic electrostrictive polymers

Next, we extend the previously discussed constitutive modeling to the case of incompressible isotropic electrostrictive polymers, which undergo large deformations and are actuated by large electric fields. Therefore, the starting point is the augmented free energy in the form

$$\Omega(\mathbf{C},\boldsymbol{\mathcal{E}}) = \Phi(\mathbf{C},\boldsymbol{\mathcal{E}}) - \frac{1}{2}\varepsilon_0\boldsymbol{\mathcal{E}}\cdot(\mathbf{C}^{-1}\cdot\boldsymbol{\mathcal{E}}). \tag{31}$$

Note, that we have taken the incompressibility condition $J = \det\mathbf{F} = 1$ into account. We replace the additive decomposition of the strain tensor used for ceramics with a multiplicative decomposition of the deformation gradient tensor into an elastic part $\mathbf{F}_e$ and an electrostrictive part $\mathbf{F}_*$ according to $\mathbf{F} = \mathbf{F}_e\cdot\mathbf{F}_*$. Then, the elastic right Cauchy-Green tensor is

$$\mathbf{C}_e = \mathbf{F}_e^T\cdot\mathbf{F}_e = \mathbf{F}_*^{-T}\cdot(\mathbf{F}^T\cdot\mathbf{F})\cdot\mathbf{F}_*^{-1} = \mathbf{F}_*^{-T}\cdot\mathbf{C}\cdot\mathbf{F}_*^{-1}. \tag{32}$$

For incompressible polymers, we require that the electrostrictive part $\mathbf{F}_*$ of the deformation gradient is in itself volume-preserving, i.e., $J = \det\mathbf{F}_* = 1$ holds. The free energy is again additively split into an elastic part Φ_e and a dielectric part Φ_d. For the elastic part we use an appropriate incompressible hyperelastic strain energy function, which depends on the elastic right Cauchy-Green tensor; e.g.

$$\Phi_\mathrm{e} = \varrho_0\phi_\mathrm{e}(\mathbf{C}_e) = \frac{\mu}{2}(\mathrm{tr}\mathbf{C}_e - 3) \tag{33}$$

for an incompressible neo-Hookean material with the Lamé parameter μ, see Bonet and Wood (2008). We note that due to the incompressibility the free energy is the same independent of which volume we refer it to, $\Phi = \varrho_0\phi = \varrho\phi$ with the free energy per unit mass ϕ. For the dielectric part of the free energy, we use the same expression as for relaxor ferroelectric ceramics, but in terms of the spatial electric field $\boldsymbol{e}$ and the spatial internal polarization $\boldsymbol{p}_\mathrm{i}$; hence, we set

$$\begin{aligned}\Phi_\mathrm{d} = -\boldsymbol{e}\cdot\boldsymbol{p} + \frac{1}{2}(\boldsymbol{p}-\boldsymbol{p}_\mathrm{i})\cdot(\varepsilon_0\boldsymbol{\chi}_0)^{-1}\\ \cdot(\boldsymbol{p}-\boldsymbol{p}_\mathrm{i}) + \Psi(\boldsymbol{p}_\mathrm{i}).\end{aligned} \tag{34}$$

With $\boldsymbol{e} = \mathbf{F}^{-T}\cdot\boldsymbol{\mathcal{E}}$, $\boldsymbol{p}_\mathrm{i} = \boldsymbol{\mathcal{P}}_\mathrm{i}\cdot\mathbf{F}^T$ and $\boldsymbol{p} = \boldsymbol{\mathcal{P}}\cdot\mathbf{F}^T$ we have

$$\begin{aligned}\Phi_\mathrm{d} = -\boldsymbol{\mathcal{E}}\cdot\boldsymbol{\mathcal{P}} + \frac{1}{2}(\boldsymbol{\mathcal{P}}-\boldsymbol{\mathcal{P}}_\mathrm{i})\cdot\mathbf{F}^T\cdot(\varepsilon_0\boldsymbol{\chi}_0)^{-1}\\ \cdot\mathbf{F}\cdot(\boldsymbol{\mathcal{P}}-\boldsymbol{\mathcal{P}}_\mathrm{i}) + \Psi(\boldsymbol{\mathcal{P}}_\mathrm{i}\cdot\mathbf{F}^T).\end{aligned} \tag{35}$$

For incompressible isotropic materials the susceptibility tensor is $\boldsymbol{\chi}_0 = \chi_0\mathbf{I}$ and the potential Ψ depends on the norm of $\boldsymbol{p}_\mathrm{i}$; the latter is $\|\boldsymbol{p}_\mathrm{i}\| = \sqrt{\boldsymbol{\mathcal{P}}_\mathrm{i}\cdot\mathbf{C}\cdot\boldsymbol{\mathcal{P}}_\mathrm{i}}$. Then

$$\begin{aligned}\Phi_\mathrm{d} = -\boldsymbol{\mathcal{E}}\cdot\boldsymbol{\mathcal{P}} + \frac{1}{2}\frac{1}{\varepsilon_0\chi_0}(\boldsymbol{\mathcal{P}}-\boldsymbol{\mathcal{P}}_\mathrm{i})\\ \cdot\mathbf{C}\cdot(\boldsymbol{\mathcal{P}}-\boldsymbol{\mathcal{P}}_\mathrm{i}) + \Psi(\|\boldsymbol{p}_\mathrm{i}\|)\end{aligned} \tag{36}$$

holds. The conditions for Ψ are analogous to Eq. (23)

$$\begin{aligned}&\|\boldsymbol{p}_\mathrm{i}\| \le p_{\mathrm{sat}},\quad \Psi'|_{\|\boldsymbol{p}_\mathrm{i}\|=0} = 0,\quad \lim_{\|\boldsymbol{p}_\mathrm{i}\|\to p_{\mathrm{sat}}}\Psi' = \infty,\\ &\Psi''|_{\|\boldsymbol{p}_\mathrm{i}\|=0} = \frac{1}{\varepsilon_0\chi_\mathrm{i}},\qquad \Psi'' \ge \frac{1}{\varepsilon_0\chi_\mathrm{i}},\end{aligned} \tag{37}$$

with the derivative Ψ' with respect to $\|\boldsymbol{p}_\mathrm{i}\|$. Again, it is sufficient to specify Ψ' rather than Ψ, as the derivatives with respect to the internal polarization and the right Cauchy-Green tensor are

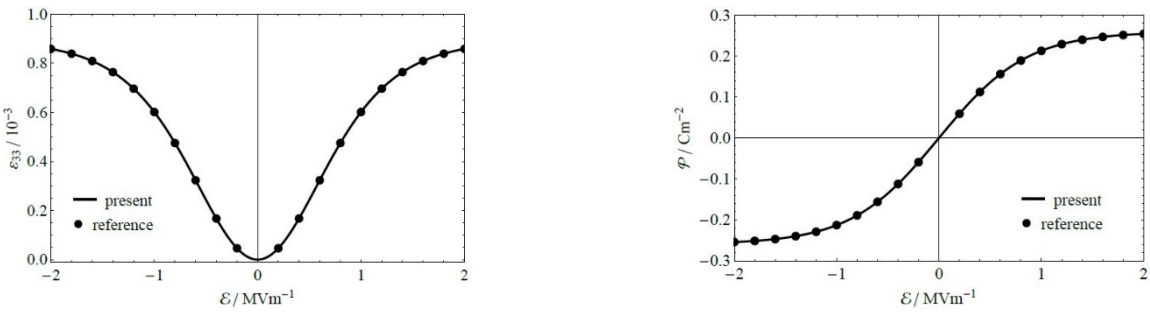

Fig. 1 Thickness strain vs. electric eld (left) and polarization vs. electric eld (right)

$$\frac{\partial \Psi}{\partial \boldsymbol{\mathcal{P}}_\mathrm{i}} = \frac{\partial \Psi}{\partial \|\boldsymbol{p}_\mathrm{i}\|}\frac{\partial \|\boldsymbol{p}_\mathrm{i}\|}{\partial \boldsymbol{\mathcal{P}}_\mathrm{i}} = \frac{1}{\|\boldsymbol{p}_\mathrm{i}\|}\Psi'\mathbf{C}\cdot\boldsymbol{\mathcal{P}}_\mathrm{i},$$
$$2\frac{\partial \Psi}{\partial \mathbf{C}} = 2\frac{\partial \Psi}{\partial \|\boldsymbol{p}_\mathrm{i}\|}\frac{\partial \|\boldsymbol{p}_\mathrm{i}\|}{\partial \mathbf{C}} = \frac{1}{\|\boldsymbol{p}_\mathrm{i}\|}\Psi'\boldsymbol{\mathcal{P}}_\mathrm{i}\boldsymbol{\mathcal{P}}_\mathrm{i}. \tag{38}$$

Therefore, the augmented free energy for an incompressible neo-Hookean material is

$$\Omega = \frac{\mu}{2}(\mathrm{tr}\mathbf{C}_e - 3) - \boldsymbol{\mathcal{E}}\cdot\boldsymbol{\mathcal{P}} + \frac{1}{2}\frac{1}{\varepsilon_0\chi_0}(\boldsymbol{\mathcal{P}} - \boldsymbol{\mathcal{P}}_\mathrm{i}) \cdot\mathbf{C}\cdot(\boldsymbol{\mathcal{P}} - \boldsymbol{\mathcal{P}}_\mathrm{i}) + \Psi(\|\boldsymbol{p}_\mathrm{i}\|) - \frac{1}{2}\varepsilon_0\boldsymbol{\mathcal{E}}\cdot(\mathbf{C}^{-1}\cdot\boldsymbol{\mathcal{E}}), \tag{39}$$

with $\mathbf{C}_e = \mathbf{F}_*^{-T}\cdot\mathbf{C}\cdot\mathbf{F}_*^{-1}, \mathbf{F}_* = \mathbf{F}_*(\boldsymbol{\mathcal{P}})$ and $\|\boldsymbol{p}_\mathrm{i}\| = \sqrt{\boldsymbol{\mathcal{P}}_\mathrm{i}\cdot\mathbf{C}\cdot\boldsymbol{\mathcal{P}}_\mathrm{i}}$. Specifying the electrostrictive deformation gradient tensor $\mathbf{F}_*$ and the potential $\Psi(\|\boldsymbol{p}_\mathrm{i}\|)$ completes the constitutive modeling. For the latter potential we use any suitable one, which must satisfy the conditions introduced in Eq. (37). For isotropic electrostrictive polymers we use

$$\Psi'(\|\boldsymbol{p}_\mathrm{i}\|) = \frac{\|\boldsymbol{p}_\mathrm{i}\|}{\left(1+\left(\frac{\|\boldsymbol{p}_\mathrm{i}\|}{p_\mathrm{sat}}\right)^n\right)^{1/n}} \tag{40}$$

with $n > 0$. As we are concerned with isotropic materials, we consider the electrostrictive part of the deformation gradient tensor to be a symmetric right stretch tensor. Let $\boldsymbol{e}_n$ denote the unit vector in the direction of material polarization, such that $\boldsymbol{\mathcal{P}} = \mathcal{P}\boldsymbol{e}_n$. Then, $\mathbf{F}_*$ is given in principal coordinates

$$\mathbf{F}_* \equiv \mathbf{U}_* = \lambda_\mathrm{el}(\mathbf{I} - \boldsymbol{e}_n\boldsymbol{e}_n) + \lambda_\mathrm{el}^{(n)}\boldsymbol{e}_n\boldsymbol{e}_n, \tag{41}$$

in which $\lambda_\mathrm{el}^{(n)}$ is the stretch in the direction of the material polarization and λ_el the stretch in any direction perpendicular to $\boldsymbol{e}_n$. These stretches are taken as functions of the square of the intensity of the polarization, $\lambda_\mathrm{el} = \lambda_\mathrm{el}(\mathcal{P}^2)$ and $\lambda_\mathrm{el}^{(n)} = \lambda_\mathrm{el}^{(n)}(\mathcal{P}^2)$. We impose incompressibility on $\mathbf{F}_*$ as $J_* = \det\mathbf{F}_* = 1$, from which

$$\det\mathbf{F}_* = 1 = \lambda_\mathrm{el}^{(n)}\lambda_\mathrm{el}^2 \quad\rightarrow\quad \lambda_\mathrm{el}^{(n)} = \lambda_\mathrm{el}^{-2} \tag{42}$$

follows, such that $\mathbf{F}_* = \lambda_\mathrm{el}(\mathbf{I} - \boldsymbol{e}_n\boldsymbol{e}_n) + \lambda_\mathrm{el}^{-2}\boldsymbol{e}_n\boldsymbol{e}_n$ holds. Different forms for λ_el are reported in the literature as functions of the intensity of the electric field; Zäh and Miehe (2015) suggested $\lambda_\mathrm{el} = (1 + (3/2)c\mathcal{E}^2)^{1/3}$, whereas Skatulla *et al*. (2012) proposed $\lambda_\mathrm{el} = e^{(c/2)\mathcal{E}^2}$ for the electric stretch. In both approaches c is an electrostrictive coeffient, which characterizes the quadratic strain response in the small strain regime, and which must be identified from experimental data. In analogy we will be using electrostrictive stretches, which depend on the square of the intensity of the polarization; in particular, we use

$$\lambda_\mathrm{el} = \left(1 + \frac{3}{2}Q\mathcal{P}^2\right)^{1/3}. \tag{43}$$

From $\mathbf{F}_*$ one can compute the corresponding Green strain tensor $2\mathbf{E}_* = \mathbf{F}_*\cdot\mathbf{F}_* - \mathbf{I}$, the linearization of which is

$$\boldsymbol{\varepsilon}^* = -\frac{3}{2}Q\left(\boldsymbol{\mathcal{P}}\boldsymbol{\mathcal{P}} - \frac{1}{3}\mathbf{I}(\boldsymbol{\mathcal{P}}\cdot\boldsymbol{\mathcal{P}})\right), \tag{44}$$

which - other than the negative sign - is identical to what we used for the ceramics. The latter negative sign comes into play due to different underlying mechanisms for electrostriction in ceramics and polymers.

2.2.1 Homogenous deformation of a disc

We discuss the homogenous deformation of a disc in a similar setup to Section 2.1.2, choosing the principal direction as $\boldsymbol{e}_3$. To this end, we first introduce the plane stress case. We assume a plane stress problem insofar as the total stress tensor is taken as $\mathbf{S} = \mathbf{S}_2$. Here, $\mathbf{S}_2$ refers to a plane perpendicular to $\boldsymbol{e}_3$ with $\boldsymbol{\mathcal{E}} = \mathcal{E}\boldsymbol{e}_3$, $\boldsymbol{\mathcal{P}} = \mathcal{P}\boldsymbol{e}_3$ and $\boldsymbol{\mathcal{P}}_\mathrm{i} = \mathcal{P}_\mathrm{i}\boldsymbol{e}_3$. Then, one can conclude that the right Cauchy-Green tensor is $\mathbf{C} = \mathbf{C}_2 + C_{33}\boldsymbol{e}_3\boldsymbol{e}_3$, in which $\mathbf{C}_2$ refers to the plane part of $\mathbf{C}$. Likewise, $\mathbf{C}_\mathrm{e} = \mathbf{C}_{2,\mathrm{e}} + C_{33,e}\boldsymbol{e}_3\boldsymbol{e}_3$ holds due to the specific form of $\mathbf{F}_*$. With these assumptions, we find the augmented free energy Ω of an incompressible and isotropic electrostrictive material as

$$\Omega = \Phi_\mathrm{e}\left(I_{\mathbf{C}_\mathrm{e}}, II_{\mathbf{C}_\mathrm{e}}\right) + \frac{1}{2}\frac{1}{\varepsilon_0\chi_0}C_{33}(\mathcal{P} - \mathcal{P}_\mathrm{i})^2 - \mathcal{E}\mathcal{P} + \Psi(|p_\mathrm{i}|) - \frac{1}{2}\varepsilon_0\frac{\mathcal{E}^2}{C_{33}}, \tag{45}$$

see Hansy-Staudigl *et al*. (2019) for dielectric elastomers and Hansy-Staudigl and Krommer (2021) for the case of an alternative formulation for electrostrictive polymers. p_i is the intensity of the spatial internal polarization, $\boldsymbol{p}_\mathrm{i} = p_\mathrm{i}\boldsymbol{e}_3$. The incompressibility condition $\det\mathbf{C} = 1$ results into $C_{33} = \det\mathbf{C}_2^{-1} = III_{\mathbf{C}_2}^{-1}$, and we find the absolute value $|p_\mathrm{i}|$ of the intensity of the spatial internal polarization as

$$|p_\mathrm{i}| = \sqrt{\boldsymbol{\mathcal{P}}_\mathrm{i}\cdot\mathbf{C}\cdot\boldsymbol{\mathcal{P}}_\mathrm{i}} = (C_{33}\mathcal{P}_\mathrm{i}^2)^{1/2} = \left(III_{\mathbf{C}_2}^{-1}\mathcal{P}_\mathrm{i}^2\right)^{1/2}. \tag{46}$$

The first two invariants of $\mathbf{C}_\mathrm{e}$ are

$$I_{\mathbf{C}_\mathrm{e}} = \lambda_\mathrm{el}^{-2}I_{\mathbf{C}_2} + \lambda_\mathrm{el}^4 III_{\mathbf{C}_2}^{-1},$$
$$II_{\mathbf{C}_\mathrm{e}} = \lambda_\mathrm{el}^{-4}\left(I_{\mathbf{C}_2}^2 - 2III_{\mathbf{C}_2}\right) + \lambda_\mathrm{el}^8 III_{\mathbf{C}_2}^{-2}, \tag{47}$$

with the two invariants $I_{\mathbf{C}_2} = \mathrm{tr}\mathbf{C}_2$ and $III_{\mathbf{C}_2} = \det\mathbf{C}_2$ of the plane part of the right Cauchy-Green tensor. Hence, for the incompressible neo-Hookean material we write the plane stress augmented free energy Ω_2 as

$$\Omega_2 = \frac{\mu}{2}\left(\lambda_\mathrm{el}^{-2}I_{\mathbf{C}_2} + \lambda_\mathrm{el}^4 III_{\mathbf{C}_2}^{-1} - 3\right) + \frac{1}{2}\frac{1}{\varepsilon_0\chi_0}III_{\mathbf{C}_2}^{-1}(\mathcal{P} - \mathcal{P}_\mathrm{i})^2 - \frac{1}{2}\varepsilon_0 III_{\mathbf{C}_2}\mathcal{E}^2 - \mathcal{E}\mathcal{P} + \Psi(|p_\mathrm{i}|), \tag{48}$$

with $|p_\mathrm{i}|$ from Eq. (46) and the electrostrictive stretch λ_el

$$\lambda_\mathrm{el} = \left(1 + \frac{3}{2}Q\mathcal{P}^2\right)^{1/3}. \tag{49}$$

The derivatives of the potential $\Psi(|p_\mathrm{i}|)$ can be derived using Eq. (46)

$$\begin{aligned}\frac{\partial\Psi}{\partial\mathcal{P}_\mathrm{i}} &= \Psi'(|p_\mathrm{i}|)\frac{1}{|p_\mathrm{i}|}III_{\mathbf{C}_2}^{-1}\mathcal{P}_\mathrm{i},\\ 2\frac{\partial\Psi}{\partial\mathbf{C}_2} &= -\Psi'(|p_\mathrm{i}|)\frac{1}{|p_\mathrm{i}|}III_{\mathbf{C}_2}^{-1}\mathbf{C}_2^{-1}\mathcal{P}_\mathrm{i}^2.\end{aligned} \tag{50}$$

Recall that $|p_\mathrm{i}| = \left(III_{\mathbf{C}_2}^{-1}\mathcal{P}_\mathrm{i}^2\right)^{1/2}$ holds and the conditions

$$\begin{aligned}&|p_\mathrm{i}| \le p_\mathrm{sat}, \quad \Psi'|_{|p_\mathrm{i}|=0} = 0, \quad \lim_{|p_\mathrm{i}|\to p_\mathrm{sat}} \Psi' = \infty,\\ &\Psi''|_{|p_\mathrm{i}|=0} = \frac{1}{\varepsilon_0\chi_\mathrm{i}}, \qquad \Psi'' \ge \frac{1}{\varepsilon_0\chi_\mathrm{i}}\end{aligned} \tag{51}$$

must be satisfied. In the plane stress case, the constitutive relations are

$$\mathbf{S}_2 = 2\frac{\partial\Omega_2}{\partial\mathbf{C}_2}, \quad D = -\frac{\partial\Omega_2}{\partial\mathcal{E}}, \quad 0 = \frac{\partial\Omega_2}{\partial\mathcal{P}}, \quad 0 = \frac{\partial\Omega_2}{\partial\mathcal{P}_\mathrm{i}}. \tag{52}$$

As a simple example, we consider a thin disc made of an electrostrictive polymer with constitutive relations as in Eq. (52) with the plane stress augmented free energy Ω_2 from Eq. (48). The disc is equipped with electrodes at its horizontal surfaces and $\boldsymbol{e}_3$ refers to the direction normal to the plane of the disc. The deformation is not constrained and no mechanical forces are applied. We denote the thickness with H and apply a voltage V between the two electrodes; hence, $\mathcal{E} = V/H$ holds. In such a problem, the resulting in-plane deformation is homogenous and characterized by a constant spherical plane right Cauchy-Green tensor. Therefore, $\mathbf{C}_2 = \lambda^2\mathbf{I}_2$ with the principal stretch λ in both in-plane directions, $\lambda_1 = \lambda_2 = \lambda$, and $\mathbf{I}_2 = \mathbf{I} - \boldsymbol{e}_3\boldsymbol{e}_3$. Moreover, the two invariants of $\mathbf{C}_2$ are

$$I_{\mathbf{C}_2} = 2\lambda^2, \quad III_{\mathbf{C}_2} = \lambda^4. \tag{53}$$

For the neo-Hookean material this results into

$$\begin{aligned}\Omega_2 = \frac{\mu}{2}&\left(2\left(\frac{\lambda}{\lambda_\mathrm{el}}\right)^2 + \left(\frac{\lambda}{\lambda_\mathrm{el}}\right)^{-4} - 3\right)\\ &+\frac{1}{2}\frac{1}{\varepsilon_0\chi_0}\lambda^{-4}(\mathcal{P}-\mathcal{P}_\mathrm{i})^2 - \frac{1}{2}\varepsilon_0\lambda^4\mathcal{E}^2\\ &-\mathcal{E}\mathcal{P} + \Psi(|p_\mathrm{i}|).\end{aligned} \tag{54}$$

Without any external force loading the problem at hand is stress free in terms of the total stress tensor, $\mathbf{S}_2 = 0$. Therefore, we derive the equilibrium condition to

$$\mathbf{S}_2 = 2\frac{\partial\Omega_2}{\partial\lambda}\frac{\partial\lambda}{\partial\mathbf{C}_2} = \frac{\partial\Omega_2}{\partial\lambda}\frac{1}{\lambda}\mathbf{I}_2 = 0, \tag{55}$$

from which we find the nonlinear relation

$$\frac{\partial\Omega_2}{\partial\lambda} = 0 = F_1(\lambda,\mathcal{E},\mathcal{P},\mathcal{P}_\mathrm{i}), \tag{56}$$

in which $\mathcal{E}$ is given. Hence, we need two more equations from the derivatives of the augmented free energy with respect to $\mathcal{P}$ and $\mathcal{P}_\mathrm{i}$, which can be written as

$$\begin{aligned}\frac{\partial\Omega_2}{\partial\mathcal{P}} &= F_2(\lambda,\mathcal{E},\mathcal{P},\mathcal{P}_\mathrm{i}) = 0,\\ \frac{\partial\Omega_2}{\partial\mathcal{P}_\mathrm{i}} &= F_3(\lambda,\mathcal{E},\mathcal{P},\mathcal{P}_\mathrm{i}) = 0.\end{aligned} \tag{57}$$

The three nonlinear equations $F_1 = 0$, $F_2 = 0$ and $F_3 = 0$ are solved for a given electric field $\mathcal{E}$ to compute λ, $\mathcal{P}$ and $\mathcal{P}_\mathrm{i}$. Then, the electric displacement can be computed from

$$D = -\frac{\partial\Omega_2}{\partial\mathcal{E}} = \varepsilon_0\lambda^4\mathcal{E} + \mathcal{P}. \tag{58}$$

It remains to identify the material parameters μ, χ_0, χ_i, Q and p_sat. For that sake, we approximate the three nonlinear relations in the vicinity of $\lambda = 1$, $\mathcal{E} = 0$, $\mathcal{P} = 0$ and $\mathcal{P}_\mathrm{i} = 0$ finding

$$\begin{aligned}&\varepsilon_{33} = -Q\mathcal{P}^2 - \frac{\varepsilon_0(1+\chi_0)}{3\mu}\mathcal{E}^2,\\ &\mathcal{P} - \mathcal{P}_\mathrm{i} = \varepsilon_0\chi_0\mathcal{E}, \quad \mathcal{P} - \mathcal{P}_\mathrm{i} = \frac{\chi_0}{\chi_\mathrm{i}}\mathcal{P}_\mathrm{i},\\ &D = \varepsilon_0\mathcal{E} + \mathcal{P};\end{aligned} \tag{59}$$

here, we have introduced the normal strain ε_{33} in thickness direction. Note that this result is independent of the actual choice of the potential Ψ, as long as the conditions given in Eq. (51) are satisfied. In the linear setting these four equations reduce to

$$\begin{aligned}&\varepsilon_{33} = -\left(\frac{\varepsilon_0(1+\chi_0)}{3\mu} + Q\varepsilon_0^2\chi^2\right)\mathcal{E}^2 = -M\mathcal{E}^2,\\ &D = \varepsilon_0(1+\chi)\mathcal{E},\end{aligned} \tag{60}$$

with the so-called apparent electrostrictive coefficient M and an apparent susceptibility $\chi = \chi_0 + \chi_\mathrm{i}$ for small electric fields. Both parameters are easily extracted from experiments or are available in the literature. Also, the shear modulus μ is typically available.

We use the material parameters for polyurethane from Diaconu *et al*. (2008), which are given in Table 2 with $\mu = Y/3$ for incompressibility; in particular, the data we use refers to sample 5 in (Diaconu *et al*. 2008). From experimental data presented as well in Diaconu *et al*. (2008), we identify the material parameters χ_0 and χ_i as $\chi_0 = 0.25\chi$ and $\chi_\mathrm{i} = 0.75\chi$, such that the electrostrictive coefficient Q can be computed to

$$Q = \frac{M - \varepsilon_0(1+\chi_0)}{\varepsilon_0^2\chi^2} = 150.25\times10^3\ \mathrm{m^4C^{-2}}. \tag{61}$$

We note that the specific choice of $\chi_0 = 0.25\chi$ has

Table 2 Material parameters for polyurethane taken from Diaconu *et al*. (2008)

$Y/\mathrm{Nm^2}$	$\chi/1$	$M/\mathrm{m^2V^{-2}}$
59.5×10^6	8.7	8.92×10^{-16}

barely no effect on Q; even for $\chi_0 = \chi$ the term

$$\frac{\varepsilon_0(1+\chi_0)}{3\mu} = 1.44 \times 10^{-18}\ \mathrm{m^4 C^{-2}} \tag{62}$$

is only 0.16% of M. First, we compute a solution from

$$\begin{aligned} \varepsilon_{33} &= -\left(\frac{\varepsilon_0(1+\chi_0)}{3\mu} + Q\varepsilon_0^2\chi^2\right)\mathcal{E}^2, \\ \mathcal{P}_\mathrm{i} &= \varepsilon_0\chi_i\mathcal{E}, \end{aligned} \tag{63}$$

which is compared to data points (extracted from Diaconu *et al*. (2008)) in the left graph of Fig. 2. Clearly, this solution captures the strain response accurately up to an electric field, which we identify as $\mathcal{E} = \mathcal{E}_\mathrm{sat} = 4.75 \times 10^6\ \mathrm{Vm^{-1}}$. The corresponding value of the internal polarization is $\mathcal{P}_\mathrm{i} = p_\mathrm{sat} = 274.41 \times 10^{-6}\ \mathrm{Cm^{-1}}$, which is indicated in the right graph of Fig. 2 by the black dots. Next, we compute a solution for the thickness strain as before up to $\mathcal{E} = \mathcal{E}_\mathrm{sat}$; for any electric field above this value, we compute the thickness strain from

$$\varepsilon_{33} = -Q(\varepsilon_0\chi_0\mathcal{E} + p_\mathrm{sat})^2 - \frac{\varepsilon_0(1+\chi_0)}{3\mu}\mathcal{E}^2, \tag{64}$$

in which we have assumed that the internal polarization above $\mathcal{E} = \mathcal{E}_\mathrm{sat}$ has saturated to the value $\mathcal{P}_\mathrm{i} = p_\mathrm{sat}$. The results are shown in Fig. 3. It can be seen that the reported experimental data for the strain response is captured very well; yet this is possible only because the internal polarization is discontinuous. Following the initial linear response, the internal polarization saturates instantenously. Above the saturation electric field, the choices $\chi_0 = 0.25\chi$ and $\chi_\mathrm{i} = 0.75\chi$ are important to capture the correct behavior.

In the geometrically nonlinear regime, we solve the nonlinear equations $F_1 = 0$, $F_2 = 0$ and $F_3 = 0$ numerically for a given electric field $\mathcal{E}$. To approximate the saturation behavior with a suitable potential $\Psi(|p_\mathrm{i}|)$, we use

$$\Psi'(|p_\mathrm{i}|) = \frac{1}{\varepsilon_0\chi_\mathrm{i}} \frac{|p_\mathrm{i}|}{\left(1 - \left(\frac{|p_\mathrm{i}|}{p_\mathrm{sat}}\right)^n\right)^{1/n}} \tag{65}$$

with $n = 10$, which satisfies the conditions of Eq. (51). We note that due to the effect of geometrical nonlinearity, the material parameters χ_0, χ_i and p_sat used in the geometrically linear regime must be adjusted. A simple curve fitting finds the full set of material parameters given in Table 3. The numerical results are presented in Fig. 4; here, we have introduced the thickness Biot strain as $\varepsilon_{33} = \lambda^{-2} - 1$. One can see that the experimental data (markers in graphs) is recovered very well in the small strain and electric field regime. Also, we recover the well known phenomena of electromechanical breakdown using the nonlinear formulation (right graph) for large electric fields. Once a critical electric field strength - the breakdown electric field - is reached, the electric field cannot be increased any more, see e.g., Xu *et al*. (2010) for dielectric elastomers and Hansy-Staudigl and Krommer (2021) for electrostrictive polymers. In our problem the breakdown field is $\mathcal{E}_\mathrm{crit,bd} = 2.593 \times 10^7\ \mathrm{Vm^{-1}}$. Finally, Fig. 5 shows the polarization and the spatial internal polarization, which exhibits the required saturation behavior.

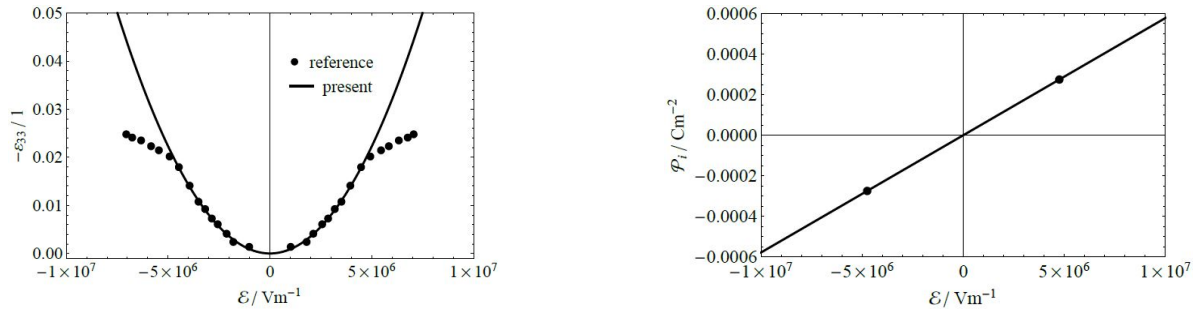

Fig. 2 Linear approximation: Thickness strain vs. electric field (left) and internal polarization vs. electric field (right)

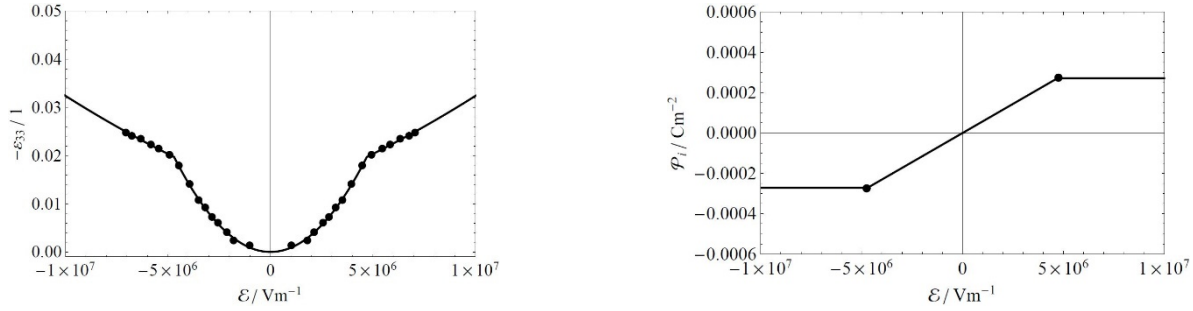

Fig. 3 Linear approximation with saturation: Thickness strain vs. electric field (left) and internal polarization vs. electric field (right)

Table 3 Full set of material parameters for polyurethane

μ/Nm^2	$\chi_0/1$	$\chi_\mathrm{i}/1$	$Q/\mathrm{m}^4\mathrm{C}^2$	$p_\mathrm{sat}/\mathrm{Cm}^{-2}$
19.83×10^6	1.566	7.134	150.25×10^3	295×10^{-6}

3. Finite element implementation

Preliminary to the discussion of the implementation of the finite element scheme to compute numerical solutions, we define the relevant physical quantities and the boundary value problem. The right Cauchy-Green tensor $\mathbf{C}=\mathbf{F}^T\cdot\mathbf{F}$ is defined in terms of the deformation gradient tensor, which is in turn defined in terms of the displacement gradient as

$$\mathbf{F}=\mathbf{I}+\nabla\boldsymbol{u}=\mathbf{F}(\boldsymbol{u}), \tag{66}$$

with the displacement vector $\boldsymbol{u}$. Above, the differential operator ∇ denotes derivatives with respect to the undeformed reference configuration. The material electric field vector is determined through the electric potential φ via

$$\boldsymbol{\mathcal{E}}=-\nabla\varphi=\boldsymbol{\mathcal{E}}(\varphi). \tag{67}$$

Therefore

$$\Omega=\Omega(\boldsymbol{u},\varphi,\boldsymbol{\mathcal{P}},\boldsymbol{\mathcal{P}}_\mathrm{i}) \tag{68}$$

holds. In the geometrically linear formulation, as $\boldsymbol{\varepsilon}=\boldsymbol{\varepsilon}(\boldsymbol{u})$, the relation $\Omega=\Omega(\boldsymbol{u},\varphi,\boldsymbol{\mathcal{P}},\boldsymbol{\mathcal{P}}_\mathrm{i})$ remains true. In case of incompressible electrostrictive polymers with the constraint $J=1$, we further add $c=-s\log(J)$ with the hydrostatic pressure s as a Lagrange multiplier to the energy expression; moreover, $J=\det\mathbf{F}=J(\boldsymbol{u})$ holds. The sum of the augmented free energy in the reference configuration and of the Lagrange term gives

$$\upsilon=\Omega(\boldsymbol{u},\varphi,\boldsymbol{\mathcal{P}},\boldsymbol{\mathcal{P}}_\mathrm{i})+c(\boldsymbol{u},s). \tag{69}$$

Now, let V denote the domain of interest and ∂V its boundary. Then, the displacement field $\boldsymbol{u}$ and the electric potential φ satisfy boundary conditions on respective boundary parts, where the body is supported or electroded

$$\boldsymbol{u}=\mathbf{0}\ \text{ on }\ \partial V_u\ \text{ and }\ \varphi=\varphi_0\ \text{ on }\ \partial V_\varphi. \tag{70}$$

To obtain the total energy functional Σ, we integrate the augmented free energy and the Lagrange term over the volume V of the reference configuration

$$\Sigma=\int_V \upsilon dV=\int_V(\Omega+c)dV. \tag{71}$$

An equilibrium point is found from the principle of virtual work

$$\delta\Sigma=\delta A^{(e)}, \tag{72}$$

with the virtual work

$$\delta A^{(e)}=\int_V \boldsymbol{b}\cdot\delta\boldsymbol{u}dV=\int_{\partial V}\boldsymbol{t}\cdot\delta\boldsymbol{u}dS \tag{73}$$

of the external body forces $\boldsymbol{b}$ and the surface tractions $\boldsymbol{t}$, and the variation

$$\delta\Sigma=\int_V\left(\frac{\partial\Omega}{\partial\boldsymbol{u}}\cdot\delta\boldsymbol{u}+\frac{\partial\Omega}{\partial\varphi}\delta\varphi+\frac{\partial\Omega}{\partial\boldsymbol{\mathcal{P}}}\cdot\delta\boldsymbol{\mathcal{P}}+\frac{\partial\Omega}{\partial\boldsymbol{\mathcal{P}}_\mathrm{i}}\cdot\delta\boldsymbol{\mathcal{P}}_\mathrm{i}+\frac{\partial c}{\partial\boldsymbol{u}}\cdot\delta\boldsymbol{u}+\frac{\partial c}{\partial s}\delta s\right)dV \tag{74}$$

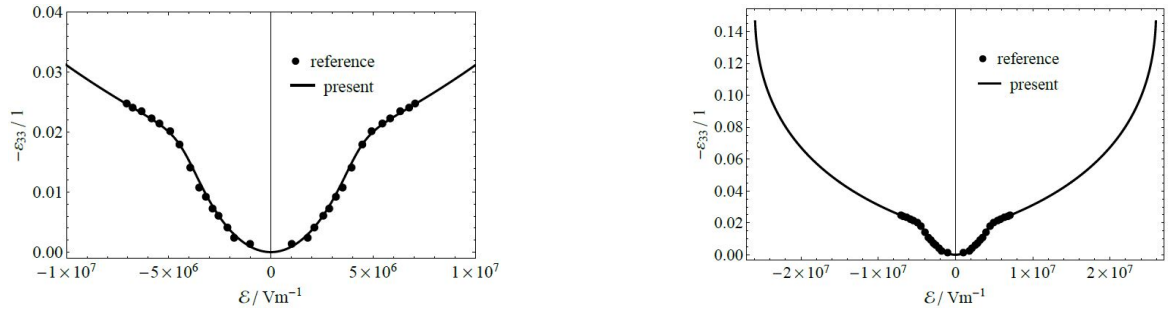

Fig. 4 Thickness strain vs. electric field for large deformations: Small electric field (left) and large electric field (right)

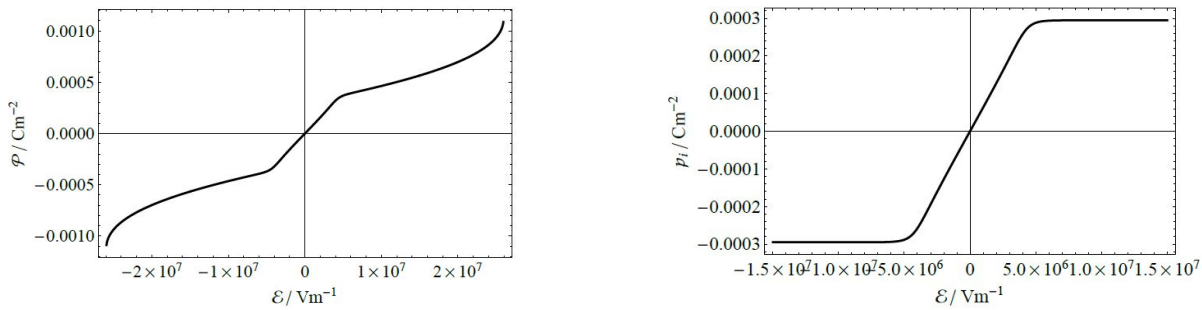

Fig. 5 Polarization (left) and internal polarization (right) vs. electric field

of the total energy functional.

3.1 Spatial finite element discretization

The above modeling approach lends itself directly to the design of a finite element method. Therefore, we assume that the volume of interest V is discretized by a regular finite element mesh $\mathcal{T} = \{T\}$ consisting of hexahedral, tetrahedral or prismatic elements T.

We consider conforming finite element approximations of the unknown fields $\boldsymbol{u}, \varphi, \boldsymbol{\mathcal{P}}$ and $\boldsymbol{\mathcal{P}}_\mathrm{i}$. Thus, we choose the displacement field $\boldsymbol{u}$ and the electric potential φ as piecewise polynomial of order k and continuous, which ensures weak differentiability, the existence of $\nabla\boldsymbol{u}$ and $\nabla\varphi$ in weak sense, and thereby finite-ness of the elastic and electric potentials

$$\boldsymbol{u} \in \{\boldsymbol{v} \in [C(V)]^3 : \boldsymbol{v}|_T \in [P^k(T)]^3,\ \boldsymbol{v} = 0 \ \text{ on } \ \partial V_u\}, \quad (75)$$

$$\varphi \in \{v \in C(V) : v|_T \in P^k(T),\ v = \varphi_0 \ \text{ on } \ \partial V_\varphi\}. \quad (76)$$

For the derived quantities $\mathbf{F}$ and $\boldsymbol{\mathcal{E}}$ the approximation order is $k-1$. When modelling incompressible materials, the hydrostatic pressure field s enters as an additional unknown. We propose to use continuous piecewise polynomial pressure fields of order $k-1$

$$s \in \{v \in C(V) : v|_T \in P^{k-1}(T)\}. \quad (77)$$

It is well known that for the above choice of $\boldsymbol{u}$ and s, we obtain a stable pair of displacement-pressure elements that go back to Taylor and Hood (1973). Polarization $\boldsymbol{\mathcal{P}}$ and internal polarization $\boldsymbol{\mathcal{P}}_\mathrm{i}$ are not necessarily differentiable, thus it is appropriate to model these quantities as piecewise polynomial without inter-element continuity conditions. Also, their order is chosen equal to that of the derived quantities, i.e., $k-1$

$$\boldsymbol{\mathcal{P}}, \boldsymbol{\mathcal{P}}_\mathrm{i} \in \{\boldsymbol{v} \in [L_2(V)]^3 : \boldsymbol{v}|_T \in [P^{k-1}(T)]^3\}. \quad (78)$$

Note that the above definition holds for tetrahedral elements only, while for hexahedral or prismatic elements the local spaces are extended to (subspaces of) $Q^k(T)$ and $Q^{k-1}(T)$ in the usual way.

Given the above finite element spaces, an approximate solution to the boundary value problem can be obtained posing the principle of virtual work, Eq. (72), for all admissible, discrete virtual displacements $\delta\boldsymbol{u}$, virtual electric potentials $\delta\varphi$, virtual (internal) polarizations $\delta\boldsymbol{\mathcal{P}}$ and $\delta\boldsymbol{\mathcal{P}}_\mathrm{i}$ and virtual pressures δs.

3.2 Numerical implementation

The finite element scheme is implemented in the open-source software package Netgen/NGSolve available at https://ngsolve.org. Netgen/NGSolve provides various types of arbitrary-order hierarchical finite elements on hybrid meshes. Moreover, the software package has a Python frontend, which allows us to symbolically define thermodynamic potentials (or their derivatives). Residual vectors and stiffness matrices are generated through automatic differentiation of these potentials. It is not necessary to compute consistent linearizations and tangent moduli by hand.

To avoid numerical breakdown near saturation, the potential $\Psi(\|\boldsymbol{p}_\mathrm{i}\|)$ is regularized as $\|\boldsymbol{p}_\mathrm{i}\| \to p_\mathrm{sat}$. We use the following regularized derivative in our computations, where $\alpha < 1$ is the regularization parameter

$$\Psi'_\alpha(\|\boldsymbol{p}_\mathrm{i}\|) = \begin{cases} \Psi'(\|\boldsymbol{p}_\mathrm{i}\|) & \text{if} \quad \|\boldsymbol{p}_\mathrm{i}\| \le \alpha p_\mathrm{sat}, \\ \big(\Psi'(\alpha p_\mathrm{sat}) + \Psi''(\alpha p_\mathrm{sat})(\|\boldsymbol{p}_\mathrm{i}\| - \alpha p_\mathrm{sat})\big) & \text{else.} \end{cases} \quad (79)$$

For $\alpha \to 1$, the above choice results in penalization for the saturation condition $\|\boldsymbol{p}_\mathrm{i}\| < p_\mathrm{sat}$. For relaxor ferroelectric ceramics, spatial and material internal polarization are not distinguished, such that in this case, $\|\boldsymbol{p}_\mathrm{i}\|$ and p_sat is replaced by $\|\boldsymbol{\mathcal{P}}_\mathrm{i}\|$ and $\mathcal{P}_\mathrm{sat}$ above.

The arising nonlinear finite element problems are solved using a Newton-Raphson iteration with linesearch. We do not observe any convergence problems for this iterative solution prodedure.

4. Examples

In this section, we present numerical results for the two types of electrostrictive materials we have discussed. The results are computed with the Finite Element scheme introduced in the section 3.

4.1 Relaxor ferroelectric ceramic PNM-PT-BT

For PMN-PT-BT with $\chi_0 = 0$ the corresponding augmented free energy is given in Eq. (19) with $\boldsymbol{\mathcal{P}} = \boldsymbol{\mathcal{P}}_\mathrm{i}$ and the electrostrictive eigenstrain is defined in Eq. (20). For the derivative of the potential $\Psi(\boldsymbol{\mathcal{P}})$ we use the one introduced in Eq. (22) with $n = 1$; hence

$$\frac{\partial\Psi}{\partial\boldsymbol{\mathcal{P}}} = \frac{\mathcal{P}_\mathrm{sat}}{\varepsilon_0\chi_\mathrm{i}} \operatorname{arctanh}\left(\frac{\|\boldsymbol{\mathcal{P}}\|}{\mathcal{P}_{sat}}\right) \frac{\boldsymbol{\mathcal{P}}}{\|\boldsymbol{\mathcal{P}}\|}. \quad (80)$$

The material parameters for the simulations are summarized in Table 4. For the Poisson ratio we have chosen $\nu = 0.4$, as it has not been given in the original paper by Hom and Shankar (1994).

4.1.1 Homogenous deformation problem

First, we re-compute the solution of the homogenous deformation problem numerically. For that sake, a homogenous cube of dimensions $a \times b \times H = 1\,\mathrm{mm} \times 1\,\mathrm{mm} \times 1\,\mathrm{mm}$ with electrodes at the top and bottom surfaces is simulated. An electric potential V is applied to the top electrode and an electric potential $-V$ to the

Table 4 Material parameters for PMN-PT-BT used in the simulations

Y/Nm^2	$\nu/1$	$Q/\mathrm{m}^4\mathrm{C}^{-2}$	$v_\mathrm{Q}/1$	$\mathcal{P}_\mathrm{sat}/\mathrm{Cm}^{-2}$	$\chi_i/1$
97×10^9	0.4	13.3×10^{-3}	0.4556	0.259	33.93×10^3

bottom electrode. Symmetry is used in the simulation, such that only 1/8 of the cube is simulated. This part includes the top surface with the applied electric potential V and the thickness center surface, which then has a zero electric potential. At those surfaces, which are actually internal surfaces of the full cube symmetry conditions are imposed. In particular, the displacement normal to these three surfaces is prohibited. In addition to the applied electric potential, we also study the case of a constant pressure p applied at the top and bottom surfaces of the (full) cube. In the simulation, the loading is realized by applying the pressure only to the top surface.

The numerical solution fully recovers the homogenous solution when using only one single linear hexahedral element, i.e., linear shape functions for the displacement field and electric potential and a constant vector-valued polarization. For this simple discretization, the analytical solution can be represented exactly by the finite element ansatz functions, which ensures that the numerical solution is indeed exact. The electric field, the polarization and the stress tensor have only a component in the thickness direction, which is constant. The strain tensor has only normal components which are constant with identical in-plane components and a thickness strain. In case a pressure is applied, the thickness strain is composed from two parts related to the pressure and the applied voltage, respectively. The numerical results for the thickness strain and the polarization are shown in Fig. 6. We define ε_{33} as the difference between the relative change of the thickness under combined electro-mechanical loading and the relative change of the thickness under purely mechanical loading

$$\varepsilon_{33} = \frac{h - H}{H} - \frac{h_p - H}{H}, \tag{81}$$

where h is the thickness in the deformed configuration under combined electro-mechanical loading, whereas h_p is the thickness in the deformed configuration resulting from the applied pressure only. We study three distinct values of applied pressure, i.e., $p = \{0, 40, 80\}$ MPa. As the FE solution recovers the homogenous solution, the presented results are in full agreement with the ones presented in Hom and Shankar (1994), which - for validation of the present formulation - are presented in the graphs as markers. A compressive pre-stress slows the increase of the polarization and, therefore, also reduces the effective actuation for a given applied electric potential.

4.1.2 Bending of a bi-morph clamped plate

In the second example we study a bi-morph plate made of two identical perfectly bonded rectangular PMN-PT-BT layers with the dimensions $a \times b \times H = 4\,\text{mm} \times 2\,\text{mm} \times 0.02\,\text{mm}$, in which H is the total thickness of the bi-morph plate, see Fig. 7. The plate is fully clamped at $x = 0$ and otherwise free; the electrode at the interface of the two layers as well as the top electrode are grounded, thus a bending actuator is obtained if an electric potential is applied at the bottom electrode. In the FE-simulation, we use an unstructured triangular in-plane mesh, which is refined geometrically towards the clamped end in two steps. Through the thickness, we use two layers of elements in each of the bi-morph layers. To avoid locking effects from using very flat elements, we choose a high element order.

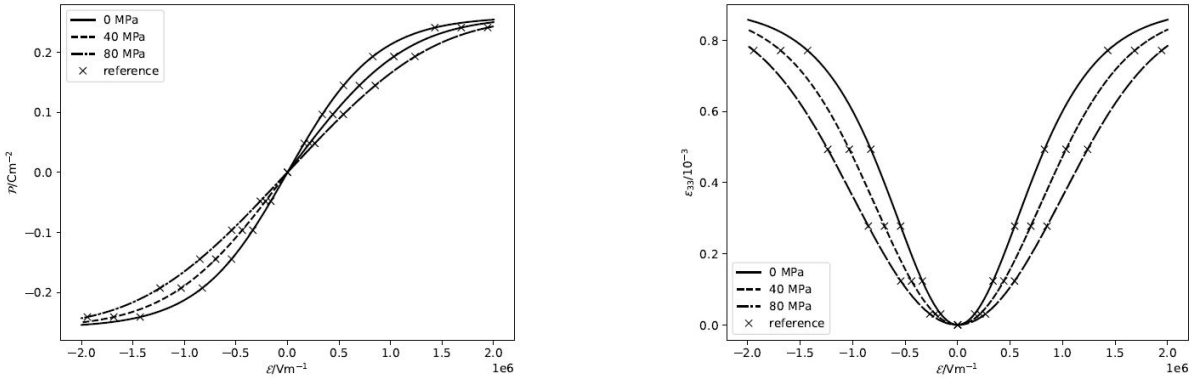

Fig. 6 Polarization vs. electric field (left) and thickness strain vs. electric field (right)

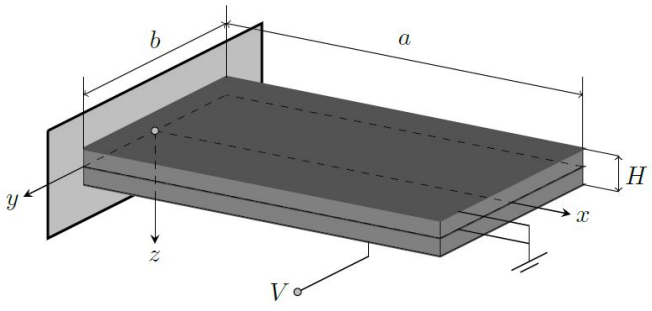

Fig. 7 Sketch of the bi-morph plate (dimensions $a \times b \times H$) fully clamped at $x = 0$; electric potential V is applied at the bottom electrode and the top electrode and the electrode at the interface are grounded

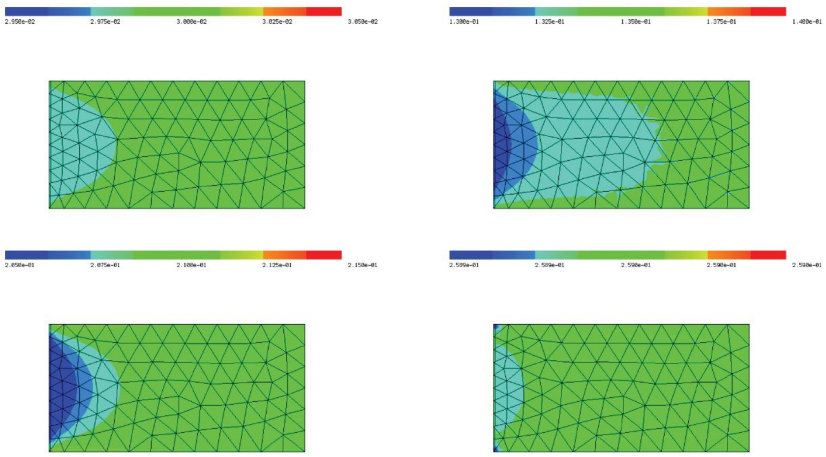

Fig. 8 Spatial distribution of the mean value of the thickness polarization for $V = \{1,5,10,40\}$ V

The displacement field and the electric potential are discretized using shape functions of order four; accordingly, the polarization is of order three. Static condensation improves the conditioning of the finite element stiffness matrix, i.e., internal degrees of freedom restricted to single elements are eliminated at assembly. Then, the stiffness matrix only contains degrees of freedom associated with displacements and electric potential at nodes located on element interfaces. For the current example, we obtain 91470 degrees of freedom that are coupling through element interfaces. A voltage of $V = 40$ V is applied in 40 load steps, none of which requires more than three Newton iterations. To avoid numerical problems close to the saturation polarization, we employ the regularization proposed in Eq. (79) with $\alpha = 1 - 10^{-10}$. The applied voltage in the bottom layer results in a positive thickness eigenstrain in the bottom layer, and, correspondingly, negative in-plane eigenstrains, which is why the plate bends downwards. The spatial distribution of the mean value of the thickness polarization in the bottom layer is shown in Fig. 8 for four voltages $V = \{1, 5, 10, 40\}$ V. Note that the color schemes are different for the different voltages. One can see that the polarization increases as the voltage increases; close to the clamping, the polarization is lower than towards the free end. Once the voltage and the corresponding electric field approach higher values, the polarization saturates to the saturation polarization $\mathcal{P}_{\mathrm{sat}}$ throughout the entire layer, which is why the resulting electrostrictive actuation saturates as well. Stress singularities at the clamped corners reduce the value of polarization at high electric fields. Saturation is also observed in Fig. 9, in which the transverse displacement of the end point at $x = a, y = 0$ m and $z = 0$ m is shown. After a quadratic increase of the deflection as a function of the applied voltage, the transverse displacement saturates as does the polarization. At $V = 40$ V, the deflection of the free end evaluates to $w = 0.2704$ mm.

4.2 Electrostrictive polymer polyurethane

We consider polyurethane as an example of an incompressible electrostrictive polymer. The elastic response is assumed to be neo-Hookean, which translates

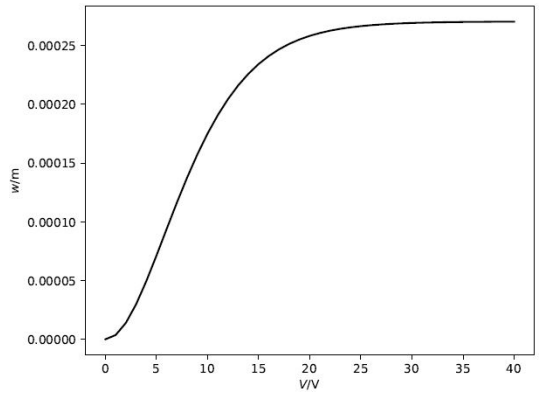

Fig. 9 Transverse displacement vs. applied voltage

into the augmented energy given in Eq. (39). The electrostrictive deformation gradient, in turn, is given by Eqs. (41) and (43), and the derivative of the potential $\Psi(\|\boldsymbol{p}_{\mathrm{i}}\|)$ is defined in Eq. (40). The material parameters are taken from Table 3.

4.2.1 Homogenous deformation problem

Again, we first solve the homogenous deformation problem of section 2.2.1 numerically. In terms of geometry, boundary conditions and loading, the problem is identical to the one we used for PMN-PT-BT. The differences lies in the augmented free energy Ω, the fact that we have two internal variables, $\boldsymbol{\mathcal{P}}$ and $\boldsymbol{\mathcal{P}}_{\mathrm{i}}$, the geometrical nonlinearity and the incompressibility. For the homogenous deformation problem, it is again sufficient to use a single hexahedral element of lowest order. Due to our choice of Taylor-Hood displacement-pressure elements, this implies an element of order two for displacement and electric potential and order one for pressure and polarizations. The numerical solution fully recovers the homogenous solution.

The applied pressure in this example problem is $p = \{0, 10, 20\}$ kPa. The numerical results for the Biot thickness strain are shown in Fig. 10. By ε_{33}, we refer to the Biot thickness strain resulting from the applied voltage only

$$\varepsilon_{33} = \frac{\lambda}{\lambda_p} - 1, \tag{82}$$

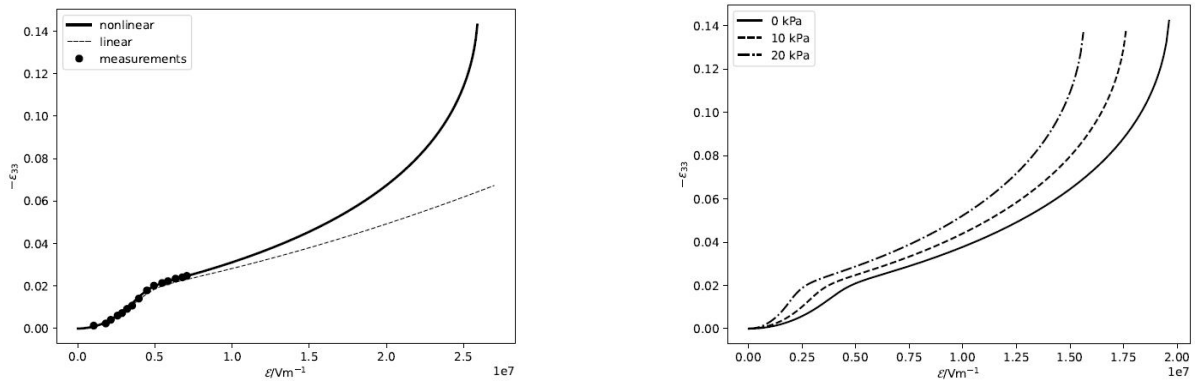

Fig. 10 Biot thickness strain vs. electric field: Without pre-stress (left) and with pre-stress (right)

where λ is the total thickness stretch and λ_p the thickness stretch induced by the pressure alone. These two thickness stretches are computed from the numerical results as

$$\lambda = 1 + \frac{w\left(\frac{H}{2}\right) - w\left(-\frac{H}{2}\right)}{H}, \qquad \lambda_p = 1 + \frac{w_p(H/2) - w_p(-H/2)}{H}. \tag{83}$$

Above, w refers to the total transverse displacement and w_p to the transverse displacement due to the pressure alone. In the left graph of Fig. 10, the strain is shown without any pre-stress, and the result from our proposed fully nonlinear formulation is compared to a result computed for a geometrically linear formulation. Besides finding the exact same result as in our previous study of this problem, one can also see that the geometrically linear solution is close to the nonlinear one up to the point at which the internal polarization saturates. Above this point, the two solutions differ significantly, and the linear solution fails to capture the electro-mechanical breakdown. For validation of our approach, we also show the measurement data from Diaconu *et al*. (2008) as circular markers. In the right graph results with pre-stress are compared to the one without pre-stress. In contrast to relaxor ferroelectric ceramics, both, the compressive pre-stress as well as the electrostrictive actuation result into a compressive thickness strain. The polarization and the internal polarization are illustrated in Fig. 11. In the left graph, we compare the nonlinear solution for the material polarization $\mathcal{P}$ with the geometrically linear solution; the two solutions are clearly very different. Concerning the internal polarization, we show the material one $\mathcal{P}_\mathrm{i}$, the spatial one p_i and the geometrically linear result. The spatial internal polarization, which saturates in our formulation, and the geometrically linear one are nearly identical. In contrast, the material internal polarization slightly increases due to geometrical nonlinearities. The right graph shows the nonlinear results with pre-stress for the material polarization. In the electrostrictive polymer, the compressive pre-stress supports the poling, i.e., the polarization and the internal polarization increase faster; therefore, the electrostrictive stretch is higher for a given electric potential, which also explains the faster increase in the actuated strain. Finally, we note that the electro-mechanical breakdown field is decreased under the presence of a compressive prestress. In order to analyze the breakdown in more detail, we compute the spatial (true) electric field at the breakdown point from

$$\boldsymbol{e} = \mathbf{F}^{-T} \cdot \boldsymbol{\mathcal{E}}. \tag{84}$$

Table 5 Material and spatial breakdown electric eld for different pre-stresses

p/kPa	0	10	20
$V_{\mathrm{crit,bd}} H^{-1}/\mathrm{Vm}^2$	$25.9 \cdot 10^6$	$24.0 \cdot 10^6$	$22.0 \cdot 10^6$
$V_{\mathrm{crit,bd}} h^{-1}/\mathrm{Vm}^2$	$30.22 \cdot 10^6$	$28.04 \cdot 10^6$	$25.51 \cdot 10^6$

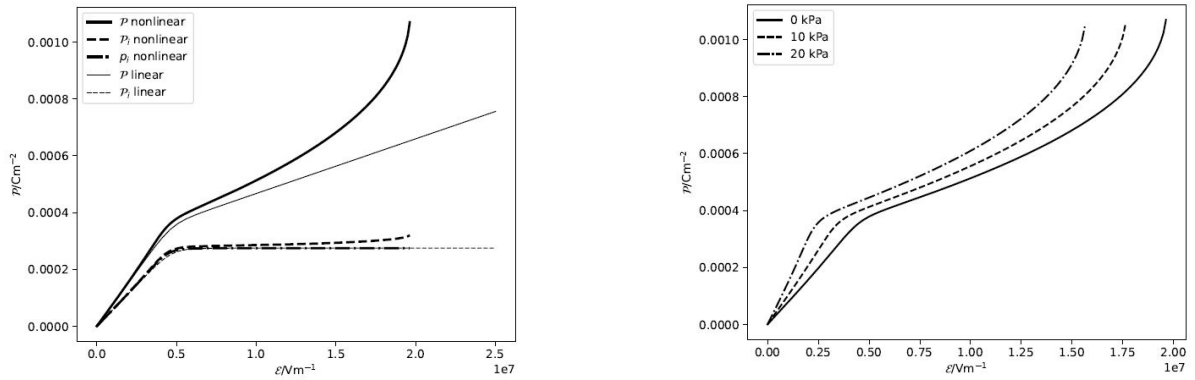

Fig. 11 Polarization & internal polarization vs. electric field: Without pre-stress (left) and with pre-stress (right)

Let $\boldsymbol{e}_3$ denote the unit vector in thickness direction, we have $\boldsymbol{\mathcal{E}} = V/H\boldsymbol{e}_3$ and therefore

$$\boldsymbol{e} = \mathbf{F}^{-T} \cdot \boldsymbol{\mathcal{E}} = \frac{V}{H}\mathbf{F}^{-T} \cdot \boldsymbol{e}_3 = \frac{V}{\lambda H}\boldsymbol{e}_3 = \frac{V}{h}\boldsymbol{e}_3 = e\boldsymbol{e}_3, \quad (85)$$

with the thickness stretch λ and the intensity e of the spatial electric field. In Table 5, the breakdown material electric field and the spatial electric field are given for $p = \{0, 10, 20\}$ kPa.

4.2.2 Bifurcation and electromechanical breakdown of a homogenous clamped plate

As a second example, we study a single layer polyurethane plate with the dimensions $a \times b \times H = 4\,\text{mm} \times 2\,\text{mm} \times 0.01\,\text{mm}$, see Fig. 12. The two opposite edges at $x = 0$ and $x = a$ are clamped in the sense that the displacement in x-direction of all nodes is prohibited.

The displacements in y-direction are free except for the points at $y = 0$, for which this displacement is prohibited, and the transverse displacement in z-direction is prohibited for $z = 0$. Otherwise, the plate is free. Conforming electrodes are attached to the top and bottom surface of the plate without taking their presence into account in the formulation; an electric potential V is applied at the top electrode and the bottom electrode is grounded. We account for symmetry and only simulate one quarter of the plate; the displacements normal to the resulting internal surfaces are prohibited.

We use a structured mesh consisting of $10 \times 4 \times 2$ hexahedral elements, using smaller mesh sizes towards the plate boundaries at $x = 0$ and $y = b/2$. We use elements of order four (fourth-order displacements and electric potential, third-order pressure and polarization), three (third-order displacements and electric potential, second-order pressure and polarization) and two (second-order displacements and electric potential, first-order pressure and polarization). This leads to 17187 coupling degrees of freedom for the fourth order elements, 8451 coupling degrees of freedom for the third order elements and 3043 coupling degrees of freedom for the second order elements. We observe rapid convergence in spite of the adverse geometric dimensions. Increasing the electric potential V at the top electrode while the bottom electrode remains grounded causes the plate to expand without any transverse displacement of the center surface $z = 0$ up to a first critical value of the electric potential, at which a supercritical pitchfork bifurcation occurs and the plate buckles out-of-plane, see the left graph of Fig. 13. The critical buckling voltage is $V_{\text{crit,buckling}} = 2.37\,\text{V}$ using elements of order three or four for the displacements and the electric potential, and it is $V_{\text{crit,buckling}} = 2.38\,\text{V}$ for elements of order two. The buckling is initiated through the choice of an unsymmetric starting configuration for the initially damped Newton iteration in each load step up to the buckling point. Still, no more than 7 iterations had to be performed in each load step. In the post buckling regime shown in the right graph of Fig. 13, the deflection increases until the applied voltage corresponds to the breakdown electric field. This instability occurs at $V_{\text{crit,bd}} = 255.5\,\text{V}$ (order 4), $V_{\text{crit,bd}} = 257.5\,\text{V}$ (order 3) and $V_{\text{crit,bd}} = 259\,\text{V}$ (order 2), to which the material electric fields

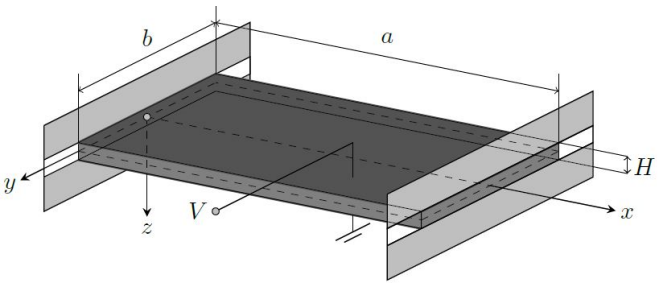

Fig. 12 Sketch of the clamped plate (dimensions $a \times b \times H$) partially clamped at $x = 0$ and $x = a$; electric potential V is applied at the top electrode and the bottom electrode is grounded

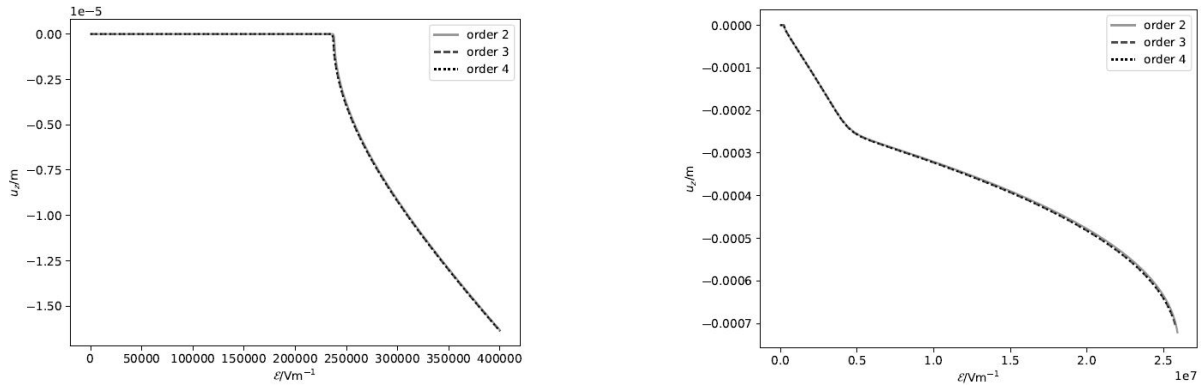

Fig. 13 Transverse displacement vs. electric field: Small electric field (left) and large electric field (right)

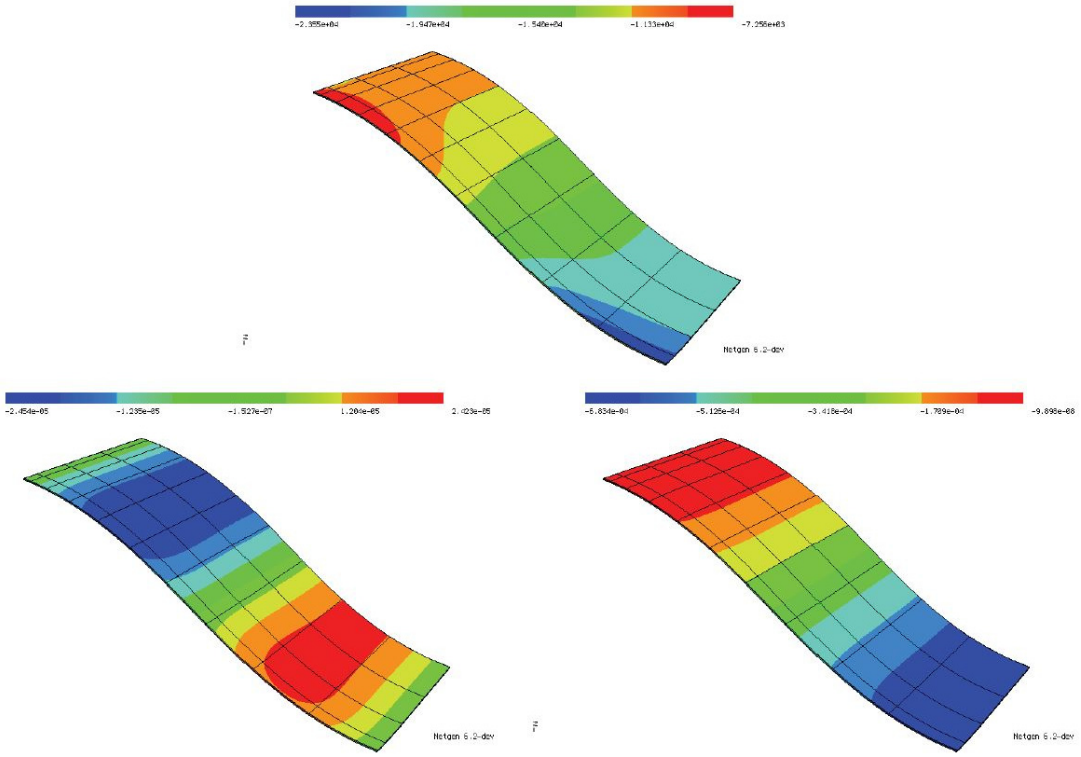

Fig. 14 Deformed conguration at $V = 255.5\ \mathrm{V}$ ishowing the hydrostatic pressure (top), the axial displacement (bottom left) and the transverse displacement (bottom right)

$\mathcal{E}_{\mathrm{crit,bd}} = 2.555 \times 10^7\ \mathrm{Vm}^{-1}$ (order 4), $\mathcal{E}_{\mathrm{crit,bd}} = 2.575 \times 10^7\ \mathrm{Vm}^{-1}$ (order 3) and $\mathcal{E}_{\mathrm{crit,bd}} = 2.59 \times 10^7\ \mathrm{Vm}^{-1}$ (order 2) correspond. The latter is the same electric field as in the homogenous deformation problem without any pre-stress. Finally, the deformed configuration of the plate is shown for $V = 255.5\ \mathrm{V}$ in Fig. 14 using elements of order 4. In addition, the hydrostatic pressure, the axial displacement and the transverse displacement of the center surface are also illustrated in these graphs.

5. Conclusions

In the present paper we have developed a geometrically and physically nonlinear theory for electrostrictive materials and structures. Constitutive modeling is based on specifying a proper form of the augmented Helmholtz free energy, in which we have introduced the polarization and an internal polarization as internal variables. The dielectric response has been decomposed into a linear part and a part by means of which we accounted for polarization saturation. The mechanical response has been decomposed into an elastic part and an inelastic part to account for electrostriction. In the geometrically nonlinear regime, the latter decomposition has been done multiplicatively for the deformation gradient tensor. Based on the augmented free energy, we have discussed and implemented an efficient Finite Element formulation that enables the simulation of thin structures made of electrostrictive ceramics and polymers. Finally, the theoretical formulation and its numerical implementation have been tested for selected example problems.

Concerning future directions, we mention the planned extension to viscoelasticity and to ferroelectricity and ferroelasticity; in particular, for the case of soft electro-active polymers undergoing large deformations. Moreover, the development of mixed Finite Elements, which are even more efficient for thin structures, and which are locking free, is currently under work.

Acknowledgments

This work has been partially supported by the Linz Center of Mechatronics (LCM) in the framework of the Austrian COMET-K2 programme.

References

Amini, A., Mohammadimehr, M. and Faraji, A. (2020), “Optimal placement of piezoelectric actuator/senor patches pair in sandwich plate by improved genetic algorithm”, *Smart Struct. Syst., Int. J.*, **26**(6), 721-733. https://doi.org/10.12989/sss.2020.26.6.721

Ask, A., Menzel, A. and Ristinmaa, M. (2012), “Phenomenological modeling of viscous electrostrictive polymers”, *Int. J. Non-Linear Mech.*, **47**, 156-165. https://doi.org/10.1016/j.ijnonlinmec.2011.03.020

Bar-Cohen, Y. (2004), *Electroactive Polymer (EAP) Actuators as Artificial Muscles: Reality, Potential, and Challenges*, SPIE Press, Bellingham, WA, USA.

Bonet, J. (2001), “Large strain viscoelastic constitutive models”, *Int. J. Solids Struct.*, **38**, 2953-2968. https://doi.org/10.1016/S0020-7683(00)00215-8

Bonet, J. and Wood, R.D. (2008), *Nonlinear Continuum Mechanics for Finite Element Analysis*, (2nd Ed.), Cambridge University Press, Cambridge, UK.

Bustamante, R. (2009), "A variational formulation for a boundary value problem considering an electro-sensitive elastomer interacting with two bodies", *Mech. Res. Commun.*, **36**, 791-795. https://doi.org/10.1016/j.mechrescom.2009.05.009

Cao, Y., Zandi, Y., Gholizadeh, M., Fu, L., Du, J., Qian, X., Wang, Z., Roco-Videla, A., Selmi, A. and Issakhov, A. (2021), "Optimization algorithms for composite beam as smart active control of structures using genetic algorithms", *Smart Struct. Syst., Int. J.*, **27**(6), 1041-1052. https://doi.org/10.12989/sss.2021.27.6.1041

Diaconu, I., Dorohoi, D.O. and Ciobanu, C. (2008), "Electromechanical response of polyurethane films with different thickness", *Roman. J. Phys.*, **53**(1-2), 91-97.

Dorfmann, A. and Ogden, R.W. (2005), "Nonlinear electroelasticity", *Acta Mechanica*, **174**, 167-183. https://doi.org/10.1007/s00707-004-0202-2

Eringen, A.C. and Maugin, G.A. (1990), *Electrodynamics of Continua I: Foundations and Solid Media*, Springer, New York, NY, USA.

Gao, Z., Tuncer, A. and Cuitiño, A.M. (2011), "Modeling and simulation of the coupled mechanical–electrical response of soft solids", *Int. J. Plasticity*, **27**(10), 1459-1470. https://doi.org/10.1016/j.ijplas.2010.07.006

Goncalves, J.F., Fonseca, J.S.O. and Silveira, O.A.A. (2016), "A controllability-based formulation for the topology optimization of smart structures", *Smart Struct. Syst., Int. J.*, **17**(5), 773-793. https://doi.org/10.12989/sss.2016.17.5.773

Hansy-Staudigl, E. and Krommer, M. (2021), "Electrostrictive polymer plates as electro-elastic material surfaces: Modeling, analysis, and simulation", *J. Intell. Mater. Syst. Struct.*, **32**(3), 296-316. https://doi.org/10.1177/1045389X20935640

Hansy-Staudigl, E., Krommer, M. and Humer, A. (2019), "A complete direct approach to nonlinear modeling of dielectric elastomer plates", *Acta Mechanica*, **230**, 3923-3943. https://doi.org/10.1007/s00707-019-02529-1

Hom, C.L. and Shankar, N. (1994), "A fully coupled constitutive model for electrostrictive ceramic materials", *J. Intell. Mater. Syst. Struct.*, **5**, 795-801. https://doi.org/10.1177/1045389X9400500610

Humer, A. and Krommer, M. (2015), "Modeling of piezoelectric materials by means of a multiplicative decomposition of the deformation gradient", *Mech. Adv. Mater. Struct.*, **22**, 125-135. https://doi.org/10.1080/15376494.2014.907948

Humer, A., Pechstein, A.S., Meindlhumer, M. and Krommer, M. (2020), "Nonlinear electromechanical coupling in ferroelectric materials: large deformation and hysteresis", *Acta Mechanica*, **231**, 2521-2544. https://doi.org/10.1007/s00707-020-02657-z

Kamlah, M. (2001), "Ferroelectric and ferroelastic piezoceramics - modeling of electromechanical hysteresis phenomena", *Continuum Mech. Thermodyn.*, **13**, 219-268.

Katsouras, I., Asadi, K., Li, M., Van Driel, T.B., Kjaer, K.S., Zhao, D., Lenz, T., Gu, Y., Blom, P.W., Damjanovic, D. and Nielsen, M.M. (2016), "The negative piezoelectric effect of the ferroelectric polymer poly(vinylidene uoride)", *Nature Mater.*, **15**, 78-84. https://doi.org/10.1038/nmat4423

Klinkel, S. (2006), "A phenomenological constitutive model for ferroelastic and ferroelectric hysteresis effects in ferroelectric ceramics", *Int. J. Solids Struct.*, **43**(22-23), 7197-7222. https://doi.org/10.1016/j.ijsolstr.2006.03.008

Klinkel, S., Zwecker, S. and Mueller, R. (2013), "A solid shell finite element formulation for dielectric elastomers", *J. Appl. Mech.*, **80**, 021026-1-021026-11. https://doi.org/10.1115/1.4007435

Lubarda, V.A. (2004), "Constitutive theories based on the multiplicative decomposition of deformation gradient: Thermoelasticity, elastoplasticity, and biomechanics", *Appl. Mech. Rev.*, **57**(4), 95-108. https://doi.org/10.1115/1.1591000

Maugin, G.A. (1988), *Continuum Mechanics of Electromagnetic Solids*, North-Holland, Amsterdam, The Netherlands.

McMeeking, R.M. and Landis, C.M. (2005), "Electrostatic forces and stored energy for deformable dielectric materials", *J. Appl. Mech.*, **72**(4), 581-590. https://doi.org/10.1115/1.1940661

Mehnert, M., Hossain, M. and Steinmann, P. (2016), "On nonlinear thermo-electro-elasticity", *Proceedings of the Royal Society A*, **472**, 20160170-1-20160170-23.

Moghadam, A.A.A., Kouzani, A., Zamani, R., Magniez, K. and Kaynak, A. (2015), "Nonlinear large deformation dynamic analysis of electroactive polymer actuators", *Smart Struct. Syst., Int. J.*, **15**(6), 1601-1623. https://doi.org/10.12989/sss.2015.15.6.1601

Mukherjee, S. and Ganguli, R. (2010), "A dragonfly inspired apping wing actuated by electro active polymers", *Smart Struct. Syst., Int. J.*, **6**(7), 867-887. https://doi.org/10.12989/sss.2010.6.7.867

Mura, T. (1987), *Micromechanics of Defects in Solids*, (2nd Ed.), Springer, Netherlands.

Pao, Y.H. (1978), "Electromagnetic forces in deformable continua", In: Nemat-Nasser S (Ed.), *Mechanics Today*, 4, Pergamon Press, Oxford, pp. 209-306.

Pechstein, A.S. (2019), "Large deformation mixed finite elements for smart structures", *Mech. Adv. Mater. Struct.*, **27**(23), 1983-1993. https://doi.org/10.1080/15376494.2018.1536932

Pechstein, A.S., Meindlhumer, M. and Humer, A. (2021), "High-order mixed finite elements for an energy-based model of the polarization process in ferroelectric materials", *J. Intell. Mater. Syst. Struct.*, **32**(3), 355-368. https://doi.org/10.1177/1045389X20953895

Pelrine, R.E., Kornbluh, R.D. and Joseph, J.P. (1998), "Electrostriction of polymer dielectrics with compliant electrodes as a means of actuation", *Sensors and Actuators A: Physical*, **64**, 77-85.

Prechtl, A. (1982a), "Eine Kontinuumstheorie elastischer Dielektrika. Teil 1: Grundgleichungen und allgemeine Materialbeziehungen", *Archiv für Elektrotechnik*, **65**(3), 167-177.

Prechtl, A. (1982b), "Eine Kontinuumstheorie elastischer Dielektrika. Teil 2: Elektroelastische und elastooptische Erscheinungen", *Archiv für Elektrotechnik*, **65**(4), 185-194.

Reissner, H. (1931), "Eigenspannungen und Eigenspannungsquellen", *Zeitschrift für Angewandte Mathematik und Mechanik*, **11**(1), 59-70.

Skatulla, S., Sansour, C. and Arockiarajan, A. (2012), "A multiplicative approach for nonlinear electro-elasticity", *Comput. Methods Appl. Mech. Eng.*, **245-246**, 243-255. https://doi.org/10.1016/j.cma.2012.07.002

Staudigl, E., Krommer, M. and Vetyukov, Y. (2018), "Finite deformations of thin plates made of dielectric elastomers: Modeling, numerics, and stability", *J. Intell. Mater. Syst. Struct.*, **29**(17), 3495-3513. https://doi.org/10.1177/1045389X17733052

Su, J., Harrison, J., Clair, T., Bar-Cohen, Y. and Leary, S. (1999), "Electrostrictive grafr elastomers and applications", *MRS Online Proceedings Library*, **600**, 131-136. https://doi.org/10.1557/PROC-600-131

Suo, Z. (2010), "Theory of dielectric elastomers", *Acta Mechanica Solida Sinica*, **23**(6), 549-578. https://doi.org/10.1016/S0894-9166(11)60004-9

Taylor, C. and Hood, P. (1973), "A numerical solution of the Navier-Stokes equations using the finite element technique", *Comput. Fluids*, **1**(1), 73-100. https://doi.org/10.1016/0045-7930(73)90027-3

Toupin, R.A. (1956), "The elastic dielectric", *J. Rational Mech. Anal.*, **5**(6), 849-915.

Vetyukov, Y., Staudigl, E. and Krommer, M. (2018), "Hybrid asymptotic-direct approach to finite deformations of electromechanically coupled piezoelectric shells", *Acta Mechanica*, **229**(2), 953-974. https://doi.org/10.1007/s00707-017-2046-6

Vu, D.K., Steinmann, P. and Possart, G. (2007), "Numerical modelling of non-linear electroelasticity", *Int. J. Numer. Methods Eng.*, **70**, 685-704. https://doi.org/10.1002/nme.1902

Xu, B.-X., Mueller,R., Klassen, M. and Gross, D. (2010), "On electromechanical stability analysis of dielectric elastomer actuators", *Appl. Phys. Lett.*, **97**, 162908. https://doi.org/10.1063/1.3504702

Yang, L., Li, X., Allahyarov, E., Taylor, P.L., Zhang, Q.M. and Zhu, L. (2013), "Novel polymer ferroelectric behavior via crystal isomorphism and the nanoconfinement effect", *Polymer*, **54**, 1709-1728. https://doi.org/10.1016/j.polymer.2013.01.035

Zäh, D. and Miehe, C. (2015), "Multiplicative electro-elasticity of electroactive polymers accounting for micromechanically-based network models", *Computat. Methods Appl. Mech. Eng.*, **286**, 394-421. https://doi.org/10.1016/j.cma.2014.12.017